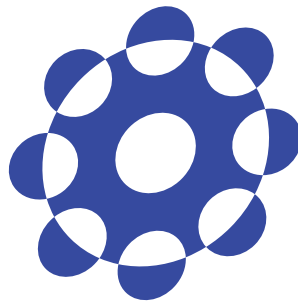# Design of Loose Spacecraft Formation Flying around Halo Orbits

Triwanto SIMANJUNTAK

In Partial Fulfillment of the Requirements
for the Degree of
Doctor of Philosophy

Department of Space and Astronautical Science
School of Physical Sciences
The Graduate University for Advanced Studies
2011

Acknowledgments

Contents

List of Figures

List of Tables

Introduction

Contents

1.1 Problem Statement

Halo orbits are periodic, three dimensional orbits which naturally exist at the collinear points, L_1, L_2, L_3, of a Circular Restricted Three Body Problem (CR3BP). Since the conception of Halo orbits in [Farquhar 1968], many deep space missions have been sent to utilized these orbits. Considering the benefits they offer, to name a few, periodicity, weak-gravity environment, constant wide access to the sky or to either of the primary bodies and also allow natural insertion to Halo orbits, there are a number of space missions being prepared and planned to use these orbits. L_2 point gives additional advantages such as stable thermal environment which is suitable for sensitive hardware, uninterrupted observations since the Sun, Earth, and Moon reside within the orbit of L_2 point. So unsurprisingly L_2 point is considered as a highly attractive location for deep space missions either employing a single spacecraft mission or in spacecraft formation flying.

Space missions at Halo orbit are mostly for observation missions and so far each mission constitute only single spacecraft. However the progress on formation flying within the last few decades has opened new possibilities of using multiple spacecraft. While thus far spacecraft formation flying mostly has been researched for Earth orbiting satellites[Scharf 2005b, Scharf 2005a] utilizing mostly the well known CW-equations [Clohessy 1960], in this thesis the possibility of implementing formation flying at Halo orbits to harvest the benefit of collinear points have to offer is attempted and examined.

1.2 Previous Contributions

Based on how the precision qualitatively enforced to the formation, we can distinguish two types of formation flying, loose formation and precise formation. A formation flying falls into precise formation category when it requires accuracy dominantly above all. Typically the precision requirement for this type of formation is

less than one meter or even much smaller. On the other hand loose formation has much less restricted precision but might demand tighter fuel cost budget. Inspecting literature thus far there are no previous works ever done on loose formation flying around halo orbits despite the huge interest spacecraft formation flying has received thus far. Most of works[Folta 2004, Roberts 2005, K. C. Howell 2003, Gill 2004] have been reported are allocated to discuss precise formation flying subjected into fuel cost optimization[Kyle T. Alfriend 2010]. It's important to consider the potential implementation of loose formation flying such as future space port concept around Halo orbits, Sun-shielded space telescopes and detached spacecraft's components (e.g. high gain antenna with pointing mechanism) to reduce structural vibration effect which inadequate if approached with the concept of precise formation. For the spaceport concept, the daughter spacecraft is admitted to move freely in the neighborhood the mother spacecraft or in the case of a Sun shielded telescope, the shield has large flexibility to move as long as it protects the telescope from the solar radiation. In the case of detached high gain antenna, provided it has accessibility to communicate with the Earth within permissible range from the mother spacecraft, the detached antenna doesn't need correction control.

1.3   Scope of Present Work

Loose formation flying may require control maneuvers to maintain and reconfigure the formation, but no strict accuracy requirements need be imposed in order for the formation to function correctly as designed. In the case of maneuvers being necessary, fuel optimization is implemented in order to achieve optimum mission life. What are particularly being considered at present are natural loose formations and artificial periodic loose formations in the vicinity of Halo orbits. In practice, the first one is definitely extreme cases since theoretical zero fuel cost is very difficult to achieve in real space missions, but it is still meaningful to examine the limitations of natural motion before addressing periodic loose formations with impulsive control. Natural loose formations are established as the product of searched out, orderly initial sets of velocities and positions, and fully rely on natural dynamics. Since searching randomly is clearly an arduous task, in this thesis a design method which allows these initial values to be found systematically and comparatively simple is proposed. While on the periodic loose formations with impulsive control, fundamentally the impulsive control is used to connect natural motions for achieving periodic relative motions. In particular the use of impulsive control from single impulse, two and three impulses are expounded in detail.

This thesis is organized as follows:

- Chapter 2: Background study is presented in this chapter. This background study includes the adoption of dynamic model of Circular Restricted Three-Body and development of tools for studying motion around Halo orbits.

- Chapter 3: Systematic design of natural loose formations is elaborated in this chapter. Modelling of the relative motion both for short-term and long-term

relative motions are explained in detailed. Further the design method and an example for natural loose formations is provided in this chapter as well.

- Chapter 4: This chapter focuses on periodic loose formations with impulsive control. Analysis on single, two and three impulses are disclosed to exemplify the design concept.

- Chapter 5: Some concluding remarks and recommended future works, from and based on this thesis are presented.

Background

Contents

2.1 Dynamical Model of Circular Restricted Three-Body Problem

Although this work is applicable to any three body problem but for the sake of clear discussion, the Sun-Earth system is adopted for all numerical computations in this paper. Perturbation forces such as solar radiation pressure (SRP), perturbation by other planets are presently ignored. Since the spacecraft is massless compared to the two primaries and the motion of the Earth (secondary primary body) relative to the Sun(first primary body) is nearly circular, then Circular Restricted Three Body Problem (CR3BP) is accurate enough to model the motion of the spacecraft (see Fig. 2.1).

In a rotating, barycentric, normalized with the Sun-Earth distance, coordinate system with the smaller primary (the Earth) on the positive x-axis, the differential equations of motion for the circular three-dimensional restricted problem are given as[Szebehely 1967]

$$\ddot{X} - 2\dot{Y} = \frac{\partial U}{\partial X} \tag{2.1}$$

$$\ddot{Y} + 2\dot{X} = \frac{\partial U}{\partial Y} \tag{2.2}$$

$$\ddot{Z} = \frac{\partial U}{\partial Z} \tag{2.3}$$

The effective potential gravity U is defined as

$$U = \frac{1}{2}\left(X^2 + Y^2\right) + \frac{1-\mu}{r_1} + \frac{\mu}{r_2}$$

$$r_1 = [(X+\mu)^2 + Y^2 + Y^2]^{\frac{1}{2}}$$

$$r_2 = [(X-1+\mu)^2 + Y^2 + Z^2]^{\frac{1}{2}} \qquad (2.4)$$

$$\mu = m_2$$

$$1 - \mu = m_1$$

$$\mu_{\text{Sun-Earth}} \approx 3.0038 \times 10^{-6}$$

X, Y, Z are coordinates with respect to the rotating frame of the spacecraft from the barycenter while m_1 and m_2 are normalized mass of the the first primary and the secondary primary bodies respectively.

2.2 Motion around Halo Orbits

2.2.1 Halo Orbits around L_2 Point

The discussion in this paper is applicable to Halo Orbits at any collinear Lagrangian points but to provide a concrete example, L_2 point is chosen. The linearized model shows that collinear point has center × center × saddle stability[Koon 2008]. However when we move to nonlinear region high enough, the unstable dynamics can be decoupled from the center dynamics hence gives us a good approximation of the dynamics in the center of manifold. In this region there exits nonlinear, 3D, periodic orbits, which in Poincare section appears to be fixed points, called Halo Orbits. As shown by Howell [Connor Howell 1984] we can find these Halo Orbits numerically by differential correction
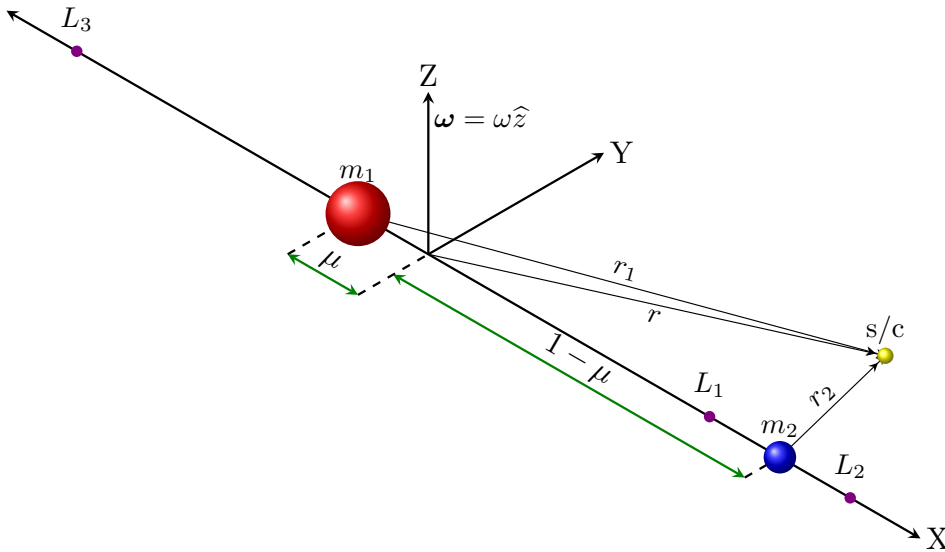
Figure 2.1: Circular Restricted Three Body Problem

method. Principally the differential correction method use Newton's method to adjust initial state vector of a reference orbit until desired accuracy achieved. The adjustment is computed numerically by making use of the State Transition Matrix (STM) of the reference orbit. The period of these orbits are approximately six months. Figures 2.2 and 2.3 show a Halo Orbit with amplitude in the Z axis, A_z, equal with $303,280\,\text{Km}$ in normalized rotating coordinate system using following initial set values, and subsequently used in all numerical computations carried here.

$$\mathbf{X}_0 = \begin{bmatrix} \mathbf{R}_0 \\ \mathbf{V}_0 \end{bmatrix} = \begin{bmatrix} 1.0112 & 0 & 0.0020 & 0 & -0.0095 & 0 \end{bmatrix}^\mathsf{T} \tag{2.5}$$
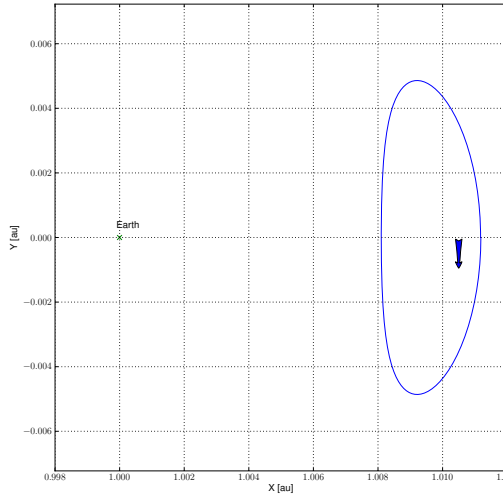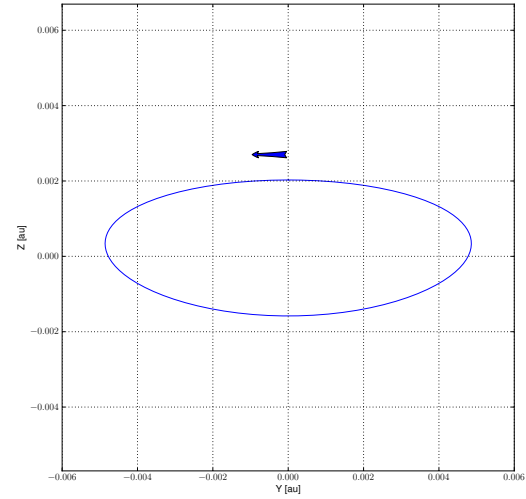
Figure 2.2: XY View   Figure 2.3: YZ View

2.2.2 The Variational Equations and the State Transition Matrix

In this subsection, variational equations which describe how perturbations evolve along a reference trajectory, assumed to be the leader's orbit, is briefly explained. As previously stated, the formation flying in our interest is in the vicinity of a Halo Orbit and since the size of the formation is much smaller than the size of the Halo orbit itself we can use the variational equations to represent the dynamics of the formation.

Equations (2.1) to (2.3) can be easily arranged in the form,

$$\dot{\mathbf{X}} = \mathbf{F}(\mathbf{X}), \qquad \mathbf{X} = \begin{bmatrix} X & Y & Z & \dot{X} & \dot{Y} & \dot{Z} \end{bmatrix}^\mathsf{T} \tag{2.6}$$

The trajectories with $\mathbf{X}(0) = \mathbf{X}_0$ is conveniently written in flow map $\phi(t; \mathbf{X}_0)$ so we can rewrite Eq. (2.6) as

$$\frac{d\phi(t; \mathbf{X}_0)}{dt} = \mathbf{F}(\phi(t; \mathbf{X}_0)) \tag{2.7}$$

where

$$\phi(t_0; \mathbf{X}_0) = \mathbf{X}_0 \tag{2.8}$$

Accordingly the relative position between the leader and the follower spacecraft in the rotating frame is simply expressed by

$$\dot{\mathbf{x}}(t) = \mathbf{F}(\phi(t; \mathbf{X}_{0_{follower}})) - \mathbf{F}(\phi(t; \mathbf{X}_{0_{leader}})) \tag{2.9}$$

with

$$\mathbf{x} = \begin{bmatrix} x & y & z & \dot{x} & \dot{y} & \dot{z} \end{bmatrix}^{\mathsf{T}} = \begin{bmatrix} \mathbf{r} \\ \mathbf{v} \end{bmatrix} \tag{2.10}$$

is the state vector of relative motion referred to reference trajectory. As the size of formation is significantly smaller than the state vector of the Halo Orbit, we can approximate the relative motions by linearization at the the leader and obtain,

$$\dot{\mathbf{x}}(t) = D\mathbf{F}(\phi(t; \mathbf{X}_{0_{leader}}))\mathbf{x}(t) = A(t)\mathbf{x}(t) \tag{2.11}$$

where,

$$
\begin{aligned}
A(t) &= \begin{bmatrix} 0 & I_3 \\ \Psi & 2\Omega \end{bmatrix} \\[6pt]
\Omega &= \begin{bmatrix} 0 & 1 & 0 \\ -1 & 0 & 0 \\ 0 & 0 & 0 \end{bmatrix} \\[6pt]
\Psi &= \begin{bmatrix} U_{xx} & U_{xy} & U_{xz} \\ U_{yx} & U_{yy} & U_{yz} \\ U_{zx} & U_{zy} & U_{zz} \end{bmatrix}
\end{aligned}
\tag{2.12}
$$

This equation obviously is a state space equation of linear time variant system, and its solution has general form known as variational equations.

$$\mathbf{x}(t) = \Phi(t, \mathbf{X}_0)\mathbf{x}_0, \qquad \Phi(t, t_0) = \frac{\partial \phi(t; \mathbf{X}_0)}{\partial \mathbf{X}_0} \tag{2.13}$$

and the State Transition Matrix, $\Phi(t, t_0)$, defined as

$$\Phi(t, t_0) = \frac{\partial \phi(t; \mathbf{X}_0)}{\partial \mathbf{X}_0} \tag{2.14}$$

In retrospect, we can see that the state transition matrix obtained for finding a Halo Orbit can be used to study the motion of the formation flying.

2.2.3   Monodromy Matrix Analysis

Monodromy matrix ($\mathbf{M}$) is basically a State-Transition Matrix (Φ) for periodic orbit which maps the state vector $\mathbf{x}_0$ at initial time t_0 to final state vector ($\mathbf{x}_T$) after one period T. This can be stated as

$$\mathbf{x}_T = \Phi(t_0 + T, \mathbf{x}_0)\mathbf{x}_0 = \mathbf{M}\mathbf{x}_0 \tag{2.15}$$

In spite of the lack of analytical expression of Halo orbits, the Monodromy matrix can be obtained numerically when the reference Halo Orbit is found. We can expect the properties of the Monodromy matrix ($\mathbf{M}$), from simple observation, due to the periodicity of the Halo orbits that its determinant has to be equal with one. The Monodromy matrix, shown in maps the initial state vectors ($\mathbf{x}_0$) to the final state ($\mathbf{x}_T$) after one period (T). Moreover its flow map from initial to final time is unknown, and neither analytical expression of the state transition matrix. However we can devise approximation of the fundamental set solutions, as elaborated in subsection 3.1 if we could establish the basis of the Monodromy matrix. This can be achieved by analyzing the independent state vector which span the space of the Monodromy matrix.

The Monodromy matrix of a Halo orbit has six eigenvalues ($\lambda_1, \lambda_2, \lambda_3, \lambda_4, \lambda_5, \lambda_6$) which can be grouped into three pairs [Gomez 2001, Koon 2008] (see Table. 2.1). The first pair (λ_1, λ_2) has self-product of one, the second pair (λ_3, λ_4) is complex conjugate with magnitude of one and the third pair (λ_5, λ_6) is real and has magnitude of one. The first pair represents stable ($\mathbf{e}_1$) and unstable manifold ($\mathbf{e}_2$), so if the initials are set in the direction of this pair's eigenvectors, the shape and the magnitude of the formation will be changed radically therefore unsuitable for establishing loosely kept formation within one period. Inspecting the other four eigenvalues reveals two modifications are needed to their eigenvectors to construct basis for the formation. Firstly, the eigenvectors ($\mathbf{e}_3, \mathbf{e}_4$) of the complex pair eigenvalues are linearly combined to form two real vectors $\mathbf{e}_{rot_{sum}} = (\mathbf{e}_3 + \mathbf{e}_4)/2$ and $\mathbf{e}_{rot_{diff}} = (\mathbf{e}_3 - \mathbf{e}_4)/2i$. Secondly since eigenvalue of one has eigenvector only one ($\mathbf{e}_5 = \mathbf{e}_6$), algebraic multiplicity is two but geometric multiplicity one, means the Monodromy matrix is defective[Marchal 1989], hence a generalized eigenvector which represents the change of energy is introduced. However the Monodromy matrix don't give us other useful information. Since the Jordan Canonical Form (JCF) provides the map of the independent eigenvectors, we could use it to look for additional valuable feature. Unfortunately the Monodromy matrix is defective so it can't be used readily because the availability of the independent vectors are less than the dimension of the state vector. To remedy this, we can use the generalized eigenvector [Strang 2003, Weintraub 2008] to find a replacement basis of the eigenvector of the eigenvalue equal with one. The generalized eigenvector ($\hat{\mathbf{e}}_6$) for λ_6 can be found by solving

$$\hat{e}_6' = \text{Ker}\left(M - \lambda_6 I\right)^2 \tag{2.16}$$

Considering that the dimension of $\hat{e}_6'$ is two, so actually any vector within the nullspace is available to choose. But it is preferable to choose a vector which have geometrical meaning therefore we select the vector ($\hat{\mathbf{e}}_6$) which lies in the nullspace and perpendicular with $\mathbf{e}_5$. Since $\mathbf{e}_5$ represents the along track direction accordingly $\hat{\mathbf{e}}_6$ represent the cross track direction. $\hat{\mathbf{e}}_6$ is found by applying Gram-Schmidt procedure to the nullspace and $\mathbf{e}_5$. The process of establishing bases in the neutrally stable manifold is shown in Figure 2.4.

Hence now we have a complete independent set of basis, which consists of three eigenvectors ($\mathbf{e}_1, \mathbf{e}_2, \mathbf{e}_5$), one generalized eigenvector ($\hat{\mathbf{e}}_6$) and two ordinary vectors which perpendicular to each other ($\mathbf{e}_{rot_{sum}}, \mathbf{e}_{rot_{diff}}$), to find the JCF. In sum the basis are:

Table 2.1: Eigenstructure of the Monodromy Matrix

	Eigenvalue
λ_1	1522
λ_2	6.572e-04
λ_3	9.789e-01+0.205i
λ_4	9.789e-01+0.205i
λ_5	1
λ_6	1

	Eigenvector
$\mathbf{e}_1$	$\begin{bmatrix} -0.374 & 0.123 & -0.022 & -0.823 & 0.393 & -0.118 \end{bmatrix}^{\mathsf{T}}$
$\mathbf{e}_2$	$\begin{bmatrix} 0.374 & 0.123 & 0.022 & -0.823 & -0.393 & -0.118 \end{bmatrix}^{\mathsf{T}}$
$\mathbf{e}_3$	$\begin{bmatrix} 0.099i & 0.509 & -0.472i & 0.500 & -0.411i & -0.300 \end{bmatrix}^{\mathsf{T}}$
$\mathbf{e}_4$	$\begin{bmatrix} -0.099i & 0.509 & 0.472i & 0.500 & 0.411i & -0.300 \end{bmatrix}^{\mathsf{T}}$
$\mathbf{e}_5$	$\begin{bmatrix} 0 & 0.670 & 0 & 0.608 & 0 & 0.429 \end{bmatrix}^{\mathsf{T}}$
$\mathbf{e}_6$	$\begin{bmatrix} 0 & 0.670 & 0 & 0.608 & 0 & 0.429 \end{bmatrix}^{\mathsf{T}}$

1. $\mathbf{e}_1$, lies in the diverging manifold, renamed $\mathbf{e}_{\text{divergence}}(\mathbf{e}_{\text{d}})$.

2. $\mathbf{e}_2$, lies in the converging manifold, renamed $\mathbf{e}_{\text{convergence}}(\mathbf{e}_{\text{c}})$.

3. $\mathbf{e}_{\text{rot}_{\text{sum}}}$ or for short $\mathbf{e}_{\text{rs}}$.
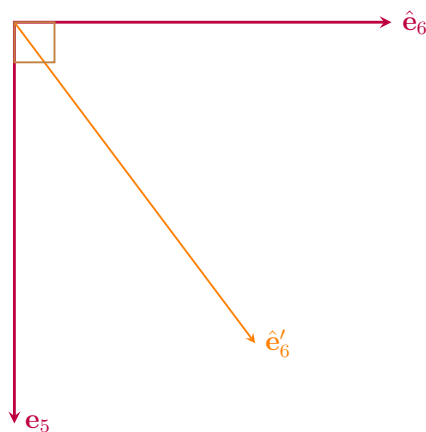
Figure 2.4: Obtaining $\hat{\mathbf{e}}_6$

4. $e_{rot_{diff}}$ or for short e_{rd}.

5. e_5, renamed $e_{along\ track}(e_{at})$ since it represents along track direction.

6. $\hat{e}_6$ renamed $e_{cross\ track}(e_{ct})$ since it represents cross track direction.

With the newly formed basis, we can establish the Jordan Canonical Form (JCF).

$$J = P^{-1}MP \tag{2.17}$$

where

$$P = \begin{bmatrix} e_d & e_c & e_{rs} & e_{rd} & e_{ct} & e_{at} \end{bmatrix} \tag{2.18}$$

The JCF is found to be in the form

$$J = \begin{bmatrix} \lambda_1 & & & & & \\ & \lambda_2 & & & & \\ & & \cos\theta & -\sin\theta & & \\ & & \sin\theta & \cos\theta & & \\ & & & & 1 & \varepsilon \\ & & & & 0 & 1 \end{bmatrix}_{6\times6} \tag{2.19}$$

where $\theta = 11.5617$ degree and $\varepsilon = -0.0255$ for the Halo orbit used above. From the Jordan Canonical Form (JCF) we can also observe that there are four Jordan blocks which represent three invariant manifolds: the stable, unstable, rotational and neutrally stable manifolds. These group manifolds give meaningful geometrical representations as previously desired. These manifolds can be grouped into subspaces:

1. The Non Periodic Subspace comprise of:

   - $E^{unstable} = \text{span}\{e_u\}$
   - $E^{stable} = \text{span}\{e_s\}$

2. The Periodic space comprise of:

   - $E^{Neutrally\ Stable} = \text{span}\{e_{at}, e_{ct}\}$
   - $E^{Rotational} = \text{span}\{e_{rs}, e_{rd}\}$

And the characteristics of these manifolds are shown in Figures 2.5 and 2.6. Based on the grouping of the manifolds above, obviously seen that in order to construct natural stable motion, we must use only the periodic subspace which spanned by only the four obtained basis. This subspace which is also known as the center manifolds allows the motion nearby a Halo orbit exclude the diverging and converging components of the natural dynamics.
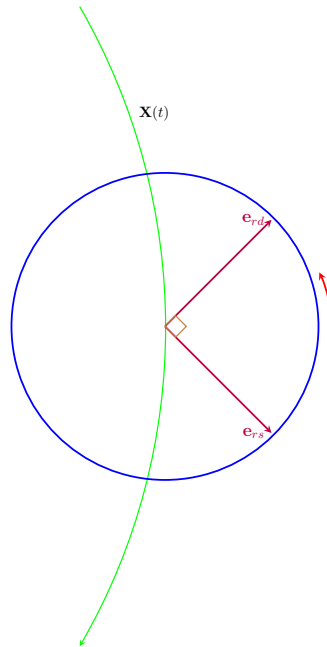
Figure 2.5: Rotational Manifold
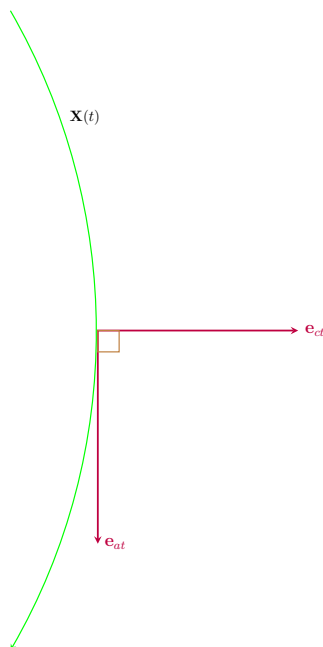
Figure 2.6: Neutrally Stable Manifold

Systematic Design of Natural Loose Formations

Contents

3.1 Modelling of the Relative Motion

3.1.1 Relative Motion Expressed with Fundamental Set Solutions

As obtained from the Monodromy matrix analysis, we have managed to establish a local coordinate system with independent directions or basis. The summary of the fundamental motions, complete basis, their eigenstructure are provided in Table 3.2. In the table the long-term motion is shown as discrete map of each basis for consecutive periods, while the short-term motion, the fundamental set solutions are shown both for in-plane and outplane motions. The fundamental set solutions basically are the propagation of the basis previously established from the Monodromy matrix. Consequently the relative motion nearby a Halo orbit reference is the linear combination of the fundamental set solutions. However we can see easily through the subspaces construction extracted from the four Jordan blocks of the Monodromy matrix, that in order to have non diverging nor converging motions, we simply need to nullify the non periodic subspaces or in other words in order to have stable motion, it must be limited within the center manifolds. Henceforth natural loose formation is designed using only four vectors, $\mathbf{e}_{rs}, \mathbf{e}_{rd}, \mathbf{e}_{at}, \mathbf{e}_{ct}$ or in other words confined within the center manifolds thus has only four degree of freedom. Subsequently in the loose formation flying the relative motion is described as,

$$\mathbf{x}(t) = \alpha \mathbf{x}_{r_s}(t) + \beta \mathbf{x}_{r_d}(t) + \gamma \mathbf{x}_{e_{at}}(t) + \kappa \mathbf{x}_{e_{ct}}(t) \tag{3.1}$$

3.1.2   Modelling Long-Term Relative Motions

Long term motion is viewed as a discrete relative motion after consecutive periods therefore can be approached from the eigenstructure of the Monodromy matrix. Moreover, the Monodromy matrix analysis has shown that we can inspect the motion in the rotational manifolds and neutrally stable manifolds independently.

It can be readily seen from the Jordan canonical form the mapping within one period as,

$$\mathbf{MP} = \mathbf{PJ} \tag{3.2}$$

This means that for the rotational manifold, we can express the rotation matrix for $n-$th period, based on its corresponding Jordan block ($\mathbf{J_R}$),

$$\mathbf{J_R} = \begin{bmatrix} \cos n\theta & -\sin n\theta \\ \sin n\theta & \cos n\theta \end{bmatrix} \tag{3.3}$$

thence the mapping after n period for rotational manifold becomes,

$$\begin{bmatrix} \mathbf{x_{rs}}(nT) & \mathbf{x_{rd}}(nT) \end{bmatrix} = \begin{bmatrix} \alpha\mathbf{x_{rs}}(0) & \beta\mathbf{x_{rd}}(0) \end{bmatrix} \mathbf{J_R} \tag{3.4}$$

thus the long term motion for the rotational manifold, obtained as

$$\begin{aligned} \mathbf{x_R}(nT) = {} & (\alpha \cos n\theta - \beta \sin n\theta)\mathbf{x_{rs}}(0) \\ & + (\alpha \sin n\theta + \beta \cos n\theta)\mathbf{x_{rd}}(0) \end{aligned} \tag{3.5}$$

While for the neutrally stable manifold the matrix transformation for $n - $ th period is given by

$$\mathbf{J_N} = \begin{bmatrix} 1 & n\varepsilon \\ 0 & 1 \end{bmatrix} \tag{3.6}$$

so we can express the mapping after $n-$ th period as

$$\begin{bmatrix} \mathbf{x_{at}}(nT) & \kappa\mathbf{x_{ct}}(nT) \end{bmatrix} = \begin{bmatrix} \gamma\mathbf{x_{at}}(0) & \kappa\mathbf{x_{ct}}(0) \end{bmatrix} \mathbf{J_N} \tag{3.7}$$

consequently the long-term motion in the neutrally stable manifold, acquired as,

$$\mathbf{x_N}(nT) = (\gamma + n\varepsilon\kappa)\mathbf{x_{ct}}(0) + \kappa\mathbf{x_{at}}(0) \tag{3.8}$$

Suitably the long-term within the center manifolds is summed as

$$\mathbf{x}(nT) = \mathbf{x_R}(nT) + \mathbf{x_N}(nT) \tag{3.9}$$

for $n = 0, 1, 2, 3, \ldots.$

3.1.3   Modelling Short-Term Relative Motions

The motion between the two spacecraft within one period its regarded as short term relative motion. Unlike the long term, the Monodromy matrix provides no information about the short term. No other mathematical tools available to model and to analyze

the formation other than numerical integration. When small displacements in the design vectors integrated numerically, as envisaged the linear behavior exhibited. This means if we can approximate the fundamental set solutions with sufficient accuracy we can combine them linearly to represent the motion within the center manifolds. As exemplified in the Table 3.2, the short term relative motions display nearly periodic behavior. This inspired us to use Fourier Series to approximate the short term relative motion. Our interest presently is mainly on the relative positions hence the approximation only carried for the position components of the fundamental set solutions. However, as illus-
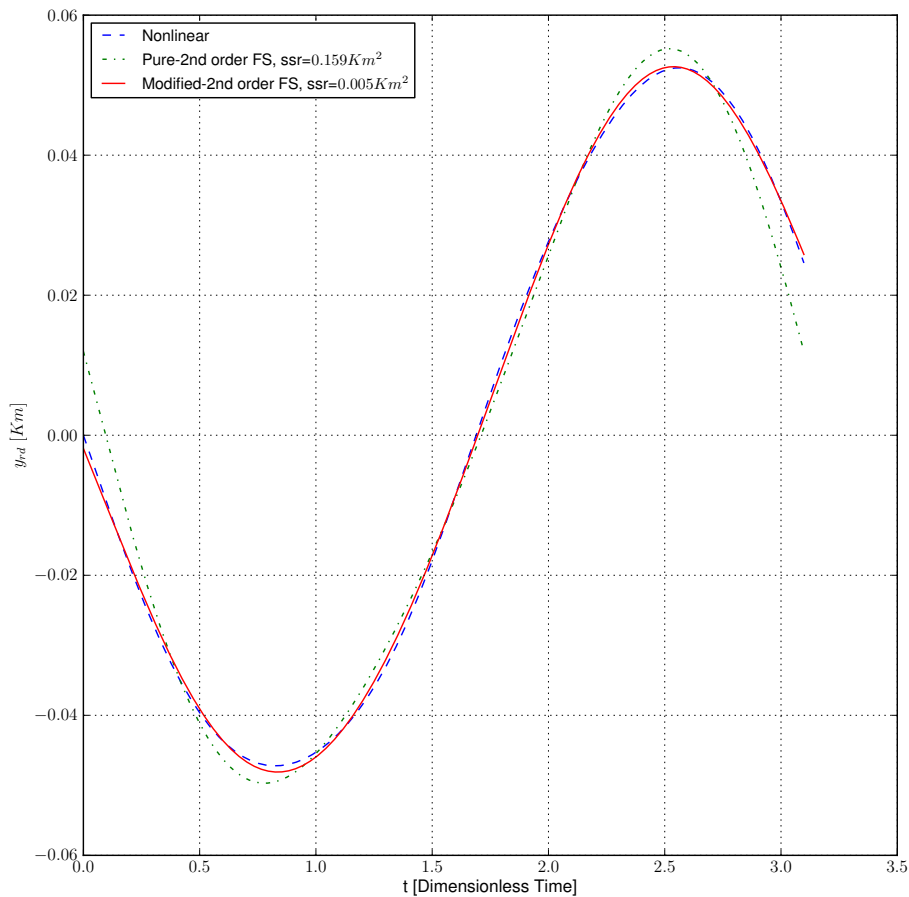

Figure 3.1: Approximation Model Comparison for y_{rd}

trated in Fig. 3.1, which uses 2nd order of pure and modified Fourier series with sample data,(m = 10000), we need to adjust pure Fourier series to accurately approximate the

motion, hence the modified Fourier series, Eq. (3.10),

$$
\widetilde{x}_{(*)}(t) = a_{0_{(*)}} + \sum_{n=1}^{n=\infty} a_{n_{(*)}} \cos(2f_n \pi \frac{t}{T})
$$
$$
+ \sum_{n=1}^{n=\infty} b_{n_{(*)}} \sin(2f_n \pi \frac{t}{T}) + c_{(*)}(\frac{t}{T})
$$

(3.10)

where $(*) = rs, rd, at, ct$, is used as general approximation model instead. As a matter of fact, full periodic behavior only displayed by motion in the direction x_{at}, for the rest of other directions, x_{rs}, x_{rd}, x_{ct}, slight modification, adding a linear function, is given to approach the motion to improve fitting accuracy of pure Fourier series . This is required due to rotational behavior within the rotational subspace for x_{rs}, x_{rd} and the influence of ε for x_{ct}. Clearly for x_{at}, the value of c is zero. The approximation is conducted by using the least-square algorithm[Strang 2003] . This algorithm used here approximates the nonlinear propagation (p_i) by minimizing the sum of squared residuals (SSR) with the approximation model ($f(q_i)$) , as described below. The summary of the approximation model is given in Table 3.1.

$$
SSR = \sum_{m=1}^{m} (p_i - f(q_i))^2
$$

(3.11)

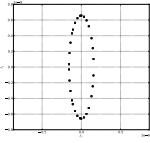Table 3.1: Approximation Model's Coefficients for Short-Term Motions
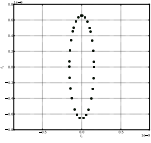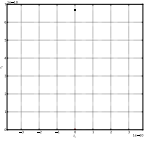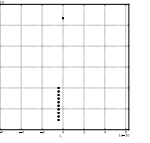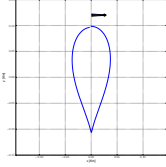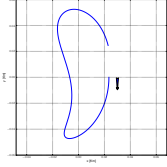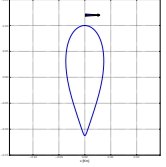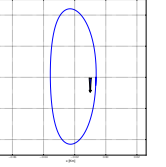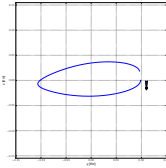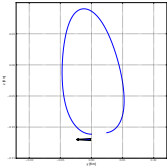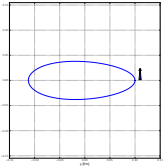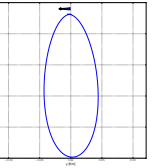
	Fourier Series Coefficients					Linear Term	Fitting Accuracy
	a_0	a_1	a_2	b_1	b_2	c	SSR
e_{rs_x}	3.48E-04	-1.20E-03	-7.51E-04	3.20E-02	1.04E-02	-5.13E-04	1.22E-02
e_{rs_y}	2.98E-04	9.91E-02	-2.90E-03	3.47E-03	1.35E-04	-2.38E-03	2.43E-02
e_{rs_z}	-7.93E-03	8.39E-03	-3.40E-04	-2.80E-02	-1.52E-03	1.82E-02	9.62E-04
e_{rd_x}	-8.20E-04	1.44E-02	8.93E-03	4.02E-03	1.30E-03	-1.93E-04	3.82E-03
e_{rd_y}	-1.40E-02	1.25E-02	-3.64E-04	-4.10E-02	-1.61E-03	2.77E-02	4.76E-03
e_{rd_z}	-1.49E-02	-2.90E-02	4.03E-03	-3.52E-03	-1.93E-04	2.29E-03	3.06E-03
e_{at_x}	-2.40E-05	-2.90E-05	-1.20E-05	3.34E-02	7.37E-03	-	1.20E-02
e_{at_y}	8.17E-06	1.04E-01	-5.74E-03	-4.51E-06	-4.00E-06	-	1.59E-01
e_{at_z}	-1.71E-07	-4.45E-06	-9.04E-07	3.81E-02	-4.46E-03	-	6.00E-03
e_{ct_x}	-1.97E-02	1.50E-02	-1.17E-03	-8.89E-04	-2.02E-04	-1.41E-04	4.68E-04
e_{ct_y}	1.77E-03	-2.66E-03	1.48E-04	-4.34E-02	5.70E-03	-3.53E-03	2.51E-03
e_{ct_z}	2.49E-02	1.14E-01	-7.96E-03	-9.59E-04	1.24E-04	6.18E-05	8.12E-03

This is due to displacements within these directions experience changing in the period. As in the true motion, then the approximated short term motion is also linear combination of the approximated fundamental set solutions, for ($0 \leq t \leq T$),

$$
\widetilde{x}(t) = \alpha \widetilde{x}_{e_{rs}}(t) + \beta \widetilde{x}_{e_{rd}}(t) + \gamma \widetilde{x}_{e_{at}}(t) + \kappa \widetilde{x}_{e_{ct}}(t)
$$

(3.12)

This approximation is valid only for the first period of the Halo orbit while for the n-th period we need to consider the influence of the long term motion. Using Eq. (3.9) and by

Table 3.2: Summary of Motions in the Center Manifolds ($\delta = 10^{-9}$)

	$e_{rot_{sum}}$	$e_{rot_{diff}}$	$e_{along\ track}$	$e_{cross\ track}$
State vector after one period	$Me_{rs} = \cos\theta\, e_{rs} - \sin\theta\, e_{rd}$	$Me_{rd} = \sin\theta\, e_{rs} + \cos\theta\, e_{rd}$	$Me_{at} = e_{at}$	$Me_{ct} = e_{ct} + \varepsilon e_{at}$
Inplane Poincare Section				
Periodic Subspace Basis	$\begin{bmatrix} 0. \\ 0.657 \\ 0. \\ 0.646 \\ 0. \\ -0.388 \end{bmatrix}$	$\begin{bmatrix} 0.157 \\ 0. \\ -0.745 \\ 0. \\ -0.649 \\ 0. \end{bmatrix}$	$\begin{bmatrix} 0. \\ 0.668 \\ 0. \\ 0.609 \\ 0. \\ 0.429 \end{bmatrix}$	$\begin{bmatrix} -0.042 \\ 0. \\ 0.879 \\ 0. \\ -0.476 \\ 0. \end{bmatrix}$
Inplane Short Term ($x_i = \delta e_i$)				
Outplane Short Term ($x_i = \delta e_i$)				

taking into account that the long term motion is a step function hence constant during the period, we can express the short term motion during the n-th cycle, ($nT \leq t \leq (n+1)T$) as

$$\widetilde{\mathbf{x}}(t') = \alpha(nT)\widetilde{\mathbf{x}}_{r_s}(t') + \beta(nT)\widetilde{\mathbf{x}}_{r_d}(nT) \\ + \gamma(nT)\widetilde{\mathbf{x}}_{e_{at}}(nT) + \kappa(nT)\widetilde{\mathbf{x}}_{e_{ct}}(t') \tag{3.13}$$

where

$$t' = t - nT \tag{3.14}$$

and considering Eq. (3.12), the approximated short term motion obtained as

$$\widetilde{\mathbf{x}}(t') = \left(\alpha\cos n\theta - \beta\sin n\theta\right)\widetilde{\mathbf{x}}_{r_s}(t') \\ + \left(\alpha\sin n\theta + \beta\cos n\theta\right)\widetilde{\mathbf{x}}_{r_d}(t') + \kappa\widetilde{\mathbf{x}}_{e_{at}}(t') \\ + \left(\gamma + n\varepsilon\kappa\right)\widetilde{\mathbf{x}}_{e_{ct}}(t') \tag{3.15}$$

As clearly seen by now, the proposed approximation allows the motion in the center of manifolds to be analyzed and be known its characteristics without have to conduct nonlinear propagation. Additionally analyzing the long term and the short term motions can be carried either simultaneously or independently in algebraic forms instead of in differential equation form, thus relatively simpler to handle in design process.

3.2 Design of Loose Natural Formations

Previously the tools needed to design loose formation flying around a Halo orbit have been constructed, so then we can sum up the design process succinctly as described in Fig. 3.2. Halo orbit is presumably computed accurately, and Monodromy matrix
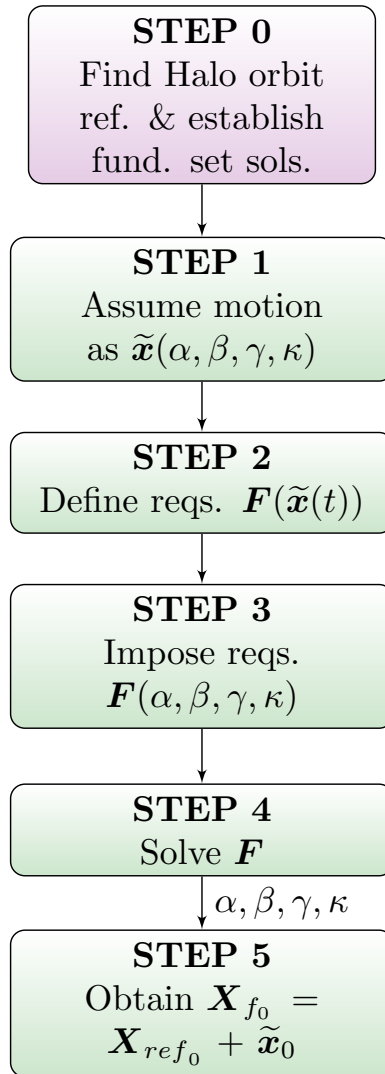
Figure 3.2: NLFF Design Chart

analysis is carried subsequently. Monodromy matrix analysis provides the basis and the fundamental set solutions is obtained by approximating the nonlinear propagation with small initial displacements along each of basis.

The design process is started by assuming the approximated relative motion, long-term and short-term, as linear combination of the basis and the fundamental set solutions accordingly. We then define the requirements the desired formation flying. These re-

quirements are expressed usually in the terms of positions or velocities. Imposing the requirements to the relative motion gives us the algebraic problems in terms of $\alpha, \beta, \gamma, \kappa$. This consequently means the design problem transformed into algebraic problems where $\alpha, \beta, \gamma, \kappa$ are design parameters. Obviously subsequently we have to solve the algebraic equations. Solving the equations will deliver the expected design parameters so finally we can acquire the initial state vectors of the desired motion with respect to the reference orbit by adding the total component of the product between corresponding design parameters with the basis.

3.3   A Design Example

As an example design, lets assume a loose formation flying contains of two spacecraft. The leader orbits the Halo orbit reference and oscillation of x-axis motion of the follower is desired and its long-term displacement in the direction of cross track need to be nullified for the first period (n = 1). This design example is resolved below in accord with the design chart in Figure 3.2

STEP 0: We use the Halo orbit, its consecutive Monodromy matrix analysis which obtained in previous sections and have the fundamental set solutions respectively.

STEP 1: The long-term and short-term motion are assumed as in Eqs. (3.9) and (3.12) respectively.

STEP 2: Based on the statement problem, we can express the formation requirements as, for long-term motion

$$F_1(\widetilde{x}(t)) = \widetilde{x}_{ct}(1*T) = 0 \tag{3.16}$$

and for short term,

$$F_2(\widetilde{x}(t)) = \widetilde{x}(t) \simeq 0 \tag{3.17}$$

STEP 3: Imposing the requirements into the assumed motions transformed the design problem into algebraic problem. Using Eq. (3.8) the long-term displacement becomes

$$F_1(\alpha, \beta, \gamma, \kappa) = \gamma + \varepsilon 1 \kappa = 0 \tag{3.18}$$

and by algebraic manipulation, we can rearrange the linear combination of the short-term motion of x-axis of the follower up to 2nd and by ignoring higher order terms (HOT) as,

$$F_2(\alpha, \beta, \gamma, \kappa) = A_o + A_1 f_1(\frac{t}{T}) + A_2 f_2(\frac{t}{T}) + A_3(\frac{t}{T}) + HOT \tag{3.19}$$

in which f_1 and f_2 are periodic functions in $\frac{t}{T}$ and

$$
\begin{aligned}
A_1 &= \left(\alpha a_{1_{x_{rs_x}}} + \beta a_{1_{x_{rd_x}}} + \gamma a_{1_{x_{at_x}}} \kappa a_{1_{x_{ct_x}}} \right)^2 \\
&\quad + \left(\alpha b_{1_{x_{rs_x}}} + \beta b_{1_{x_{rd_x}}} + \gamma b_{1_{x_{at_x}}} \kappa b_{1_{x_{ct_x}}} \right)^2 \\
&= 0 \\
A_2 &= \left(\alpha a_{2_{x_{rs_x}}} + \beta a_{2_{x_{rd_x}}} + \gamma a_{2_{x_{at_x}}} \kappa a_{2_{x_{ct_x}}} \right)^2 \\
&\quad + \left(\alpha b_{2_{x_{rs_x}}} + \beta b_{2_{x_{rd_x}}} + \gamma b_{2_{x_{at_x}}} \kappa b_{2_{x_{ct_x}}} \right)^2 \\
&= 0
\end{aligned}
\tag{3.20}
$$

STEP 4: Solving F_1 gives, the relation between κ, γ must be in the form

$$
\gamma = -\varepsilon \kappa
\tag{3.21}
$$

and If we are interested to suppress the oscillation up to 2nd so we can ignore high order term, order then formation requirement for short-term motion,

$$
f_1 = f_2 = 0
\tag{3.22}
$$

Considering Eqs. (3.20) and (3.21) we see system of equations of one degree of freedom. So we can either define the value of κ or γ and then solve the equations simultaneously. Say we choose $\kappa = 1$, then $\gamma = -\varepsilon$ and then consequently we can solve Eq. (3.22) numerically. The optimized results are obtained as $\alpha, \beta = 0.10562765, -0.63046903$. These results are not exact solutions since Eq. (3.22) gives four equations to be solved hence the total number of equations exceed the number of variables.

STEP 5: With the complete set of $\alpha, \beta, \gamma, \kappa$ we can easily find the initial state vector of the follower. As expected in Fig. (3.3), the nonlinear propagation shows suppressed motion in x direction. The solution also results suppressed motion in y direction. Furthermore Fig. (3.4) illustrates how the resulted has dominant motion in z direction compared with the in-plane motion.

$$
\widetilde{\mathbf{x}}_0 = \alpha \mathbf{x}_{0_{ers}} + \beta \mathbf{x}_{0_{erd}} + \gamma \mathbf{x}_{0_{eat}} + \kappa \mathbf{x}_{0_{ect}}
\tag{3.23}
$$

so we can have the initial state vector of the follower as,

$$
\mathbf{X}_f = \mathbf{X}_{ref_0} + \widetilde{\mathbf{x}}_0
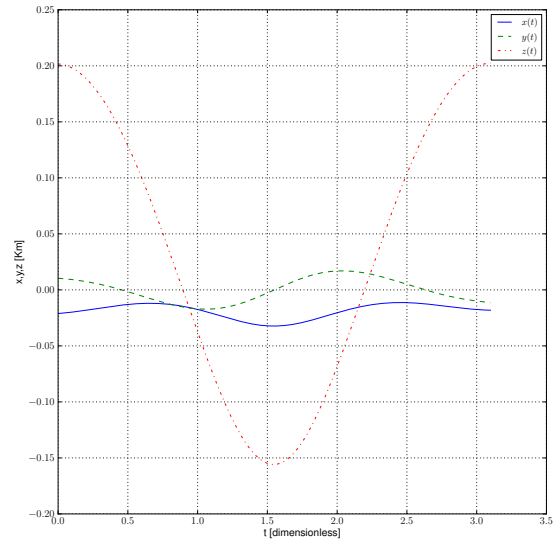\tag{3.24}
$$

Figure 3.3: Motion with Suppressed x(t)
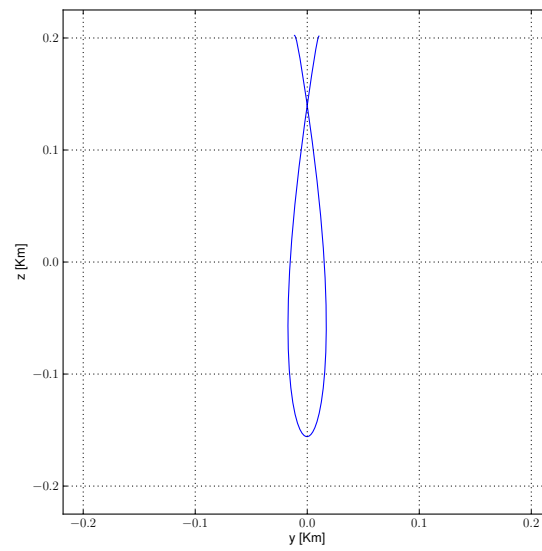
Figure 3.4: Outplane Motion of the Follower

Systematic Design of Periodic Loose Formations with Impulsive Control

Contents

4.1 Design of Loose Formation with Impulsive Control

Periodic motions are not only mathematically interesting but also very useful in orbit design for space missions either for Earth satellites or for deep space missions. Periodic motions provide predictability and regularity in position and velocity which allow us to construct useful applications such as orbits for remote sensing, scientific observations, guidance and navigation, communication and broadcasting, and military. Periodic relative motions in the vicinity of Halo orbits, as previously explained, can be used to achieve loose formations. However, as explained in Chapter 3, natural motions in the vicinity of Halo orbits provides only one design's degree freedom, along-track direction, for periodic relative motions. This lack of design degree of freedom is too restrictive in designing the loose formations and gives less space for mission designers. To remedy this problem, control maneuvers are introduced to the dynamics to expand design's

This chapter elaborates the use of impulsive control to achieve artificial periodic motions. The impulsive control in this study is assumed to change the dynamics instantly. The basic idea of artificial periodic motions with impulsive control is to change the natural motion into from one state into another state. In other words, the impulsive control connect two or more different natural motions to form cyclical motions.

Figure 4.1 illustrates the schematic of artificial periodic motions with impulsive control. In the figure n trajectories are connected at τ_i by n impulsive control. The schematic
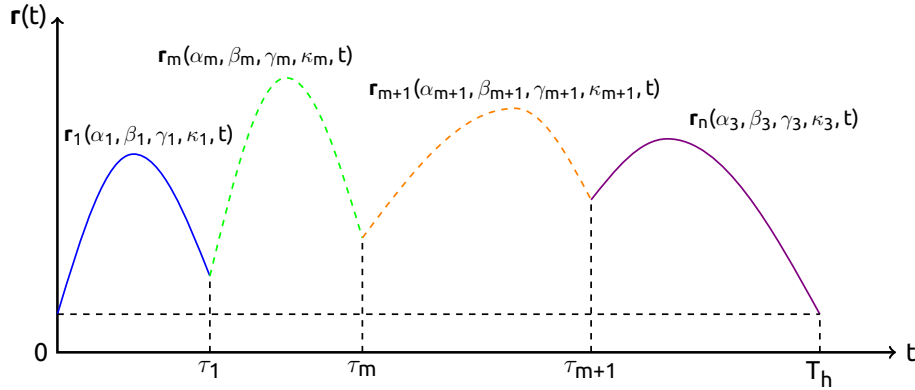
Figure 4.1: N Impulsive Control Schematic

requires the position at the connecting points must be the same and the position after one period must return to the origin. The position requirements comprises of inner condition,

$$\mathbf{r}_m(\tau_m) = \mathbf{r}_{m+1}(\tau_m), \tag{4.1}$$

where

$$m = 1, 2, 3, \ldots, n-1, \tag{4.2}$$

and initial/terminal condition,

$$\mathbf{r}_1(0) = \mathbf{r}_n(T_h). \tag{4.3}$$

The inner condition yields $3(n-1)$ equations while the initial/terminal conditions supply three equations, hence in total Eq. 4.1 and Eq. 4.3 give $3n$ equations. As the number of trajectory to be connected increases we expect to gain additional design's degree of freedom. It has been established previously that motions in the center manifolds are defined by the four parameters,

$$\mathbf{r}_n = \mathbf{r}_n(\alpha_n, \beta_n, \gamma_n, \kappa_n), \tag{4.4}$$

so for m trajectories, are to be connected by imposing Eq. 4.1 and Eq. 4.3, theoretically the number of design's DOF becomes,

$$DOF = 4n - 3n = n, \tag{4.5}$$

Or in other words, the number of expected design's DOF is equal with the number of impulses.

While the velocities required for control maneuvers are easily found by inspecting the velocity differences at each connecting points or the amount of $\Delta\mathbf{v}$ to be given at each impulse,

$$\Delta v_m = |\mathbf{v}_{m+1} - \mathbf{v}_m|, \tag{4.6}$$

$$\Delta v_n = |\mathbf{v}_n - \mathbf{v}_0|, \tag{4.7}$$

and the total Δv per cycle is the sum of all Δv_n,

$$\Delta v_{total} = \sum_1^n \Delta v_m. \tag{4.8}$$

In the following sections, the systematic design is applied and elaborated for single, double and triple impulses. Additionally generalization for N Impulses is also made available.

4.2 Single Impulse Periodic Relative Motions

Based on Section 4.1, the schematic for single impulse periodic loose formation is illustrated in Figure 4.2. It's easy to see that for single impulse only initial/terminal condition is necessary as the number of trajectory is only one. Using Eq. 4.3 for single impulse
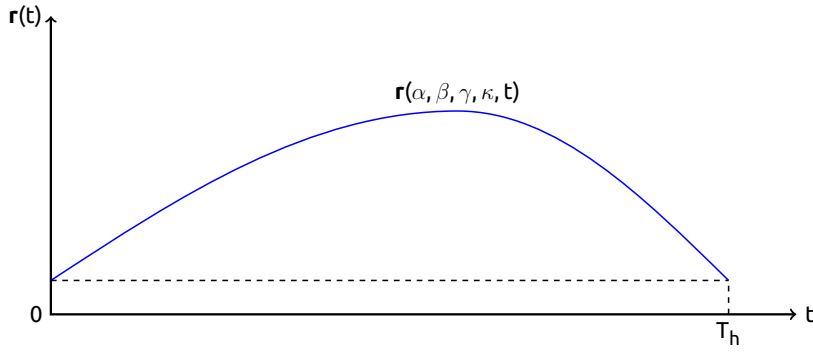
Figure 4.2: Single Impulsive Control Schematic

case produces,

$$\mathbf{r}_1(0) = \mathbf{r}_2(T), \tag{4.9}$$

which in detail provides,

$$\begin{aligned}
\alpha \mathbf{r}_{rs}(0) + \beta \mathbf{r}_{rd}(0) + \gamma \mathbf{r}_{at}(0) + \kappa \mathbf{r}_{ct}(0) = \\
\alpha \mathbf{r}_{rs}(T_h) + \beta \mathbf{r}_{rd}(T_h) + \gamma \mathbf{r}_{at}(T_h) + \kappa \mathbf{r}_{ct}(T_h).
\end{aligned} \tag{4.10}$$

The relationship between initial and terminal positions is described by Eq. 3.10, by providing $t = T_h$,

$$\begin{aligned}
\mathbf{r}_{at}(T_h) &= \mathbf{r}_{at}(0), \\
\mathbf{r}_{rs}(T_h) &= \mathbf{r}_{rs}(0) + \mathbf{c}_{rs}, \\
\mathbf{r}_{rd}(T_h) &= \mathbf{r}_{rd}(0) + \mathbf{c}_{rd}, \\
\mathbf{r}_{ct}(T_h) &= \mathbf{r}_{ct}(0) + \mathbf{c}_{ct},
\end{aligned} \tag{4.11}$$

then equations 4.10 and 4.11 is reduced into,

$$\alpha \mathbf{c}_{rs} + \beta \mathbf{c}_{rd} + \kappa \mathbf{c}_{ct} = 0, \tag{4.12}$$

which can be written in matrix form as,

$$
\underbrace{\begin{bmatrix} c_{rs_x} & c_{rd_x} & c_{ct_x} \\ c_{rs_y} & c_{rd_y} & c_{ct_y} \\ c_{rs_z} & c_{rd_z} & c_{ct_z} \end{bmatrix}}_{\mathbf{A_1}} \underbrace{\begin{bmatrix} \alpha \\ \beta \\ \kappa \end{bmatrix}}_{\mathbf{p_1}} = 0, \tag{4.13}
$$

or simplified as

$$
\mathbf{A_1 p_1} = 0. \tag{4.14}
$$

Inspecting the equation above, obviously seen that the trivial solution is,

$$
\begin{aligned} \alpha = \beta = \kappa = 0, \\ \gamma \equiv \text{free parameter.} \end{aligned} \tag{4.15}
$$

This trivial solution implies when the initial relative motion is kept to have only component in the along-track direction, single impulse periodic motion is achieved with $\Delta v = 0$. Or in other word, the introduction of single impulse into the dynamics, the number of design's DOF as expected is one, γ. The value of γ can be chosen freely to meet the size of the formations as desired. This also reinforce the knowledge revealed in natural formations that along-track direction is periodic. On the other hand nontrivial solution, generally is not available since in most cases the determinant of $\mathbf{A_1}$ aren't zero. The value of the matrix depends on the Halo orbit chosen as reference. If a periodic relative motion is desired, then clearly the orbit reference must be searched to comply with the determinant requirement.

4.3 Two Impulses Artificial Periodic Relative Motions

As detailed in Section 4.1, the schematic for two impulses case can be constructed as in Figure. 4.3. In two impulses case, there are two trajectories connected by employing the
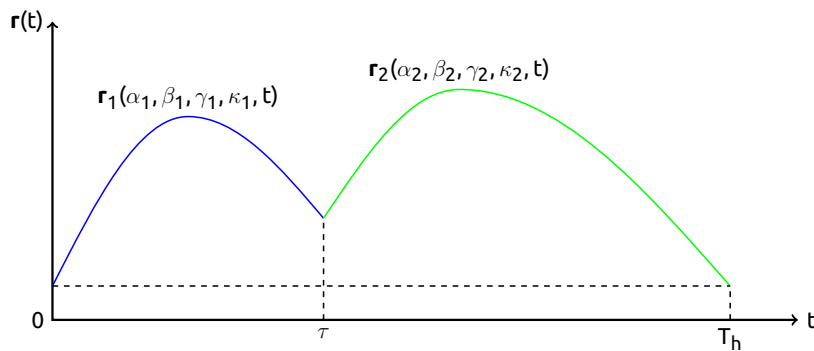

Figure 4.3: Two Impulsive Control Schematic

first impulse at τ and the second impulse at T_h. Evaluating Eq. 4.1 and Eq. 4.3 give,

$$
\begin{aligned} \mathbf{r_2}(T_h) = \mathbf{r_1}(0), \\ \mathbf{r_2}(\tau_1) = \mathbf{r_1}(\tau_1), \end{aligned} \tag{4.16}
$$

when expanded yields,

$$\alpha_2 \mathbf{r}_{rs}(T_h) + \beta_2 \mathbf{r}_{rd}(T_h) + \gamma_2 \mathbf{r}_{at}(T_h) + \kappa_2 \mathbf{r}_{ct}(T_h)$$
$$-(\alpha_1 \mathbf{r}_{rs}(0) + \beta_1 \mathbf{r}_{rd}(0) + \gamma_1 \mathbf{r}_{at}(0) + \kappa_1 \mathbf{r}_{ct}(0)) = 0 \tag{4.17}$$

and

$$\alpha_2 \mathbf{r}_{rs}(\tau) + \beta_2 \mathbf{r}_{rd}(\tau) + \gamma_2 \mathbf{r}_{at}(\tau) + \kappa_2 \mathbf{r}_{ct}(\tau)$$
$$-(\alpha_1 \mathbf{r}_{rs}(\tau) + \beta_1 \mathbf{r}_{rd}(\tau) + \gamma_1 \mathbf{r}_{at}(\tau) + \kappa_1 \mathbf{r}_{ct}(\tau)) = 0. \tag{4.18}$$

Equation. 4.18, can be rewritten as,

$$(\alpha_2 - \alpha_1)\mathbf{r}_{rs}(\tau) + (\beta_2 - \beta_1)\mathbf{r}_{rd}(\tau) + (\gamma_2 - \gamma_1)\mathbf{r}_{at}(\tau) + (\kappa_2 - \kappa_1)\mathbf{r}_{ct}(\tau) = 0 \tag{4.19}$$

and with Eq. 4.11, also can be rearranged as,

$$(\alpha_2 - \alpha_1)\mathbf{r}_{rs}(0) + (\beta_2 - \beta_1)\mathbf{r}_{rd}(0) + (\gamma_2 - \gamma_1)\mathbf{r}_{at}(0) + (\kappa_2 - \kappa_1)\mathbf{r}_{ct}(0)$$
$$+\alpha_2 \mathbf{c}_{rs} + \beta_2 \mathbf{c}_{rd} + \gamma_2 \mathbf{0} + \kappa_2 \mathbf{c}_{ct} = 0 \tag{4.20}$$

By defining,

$$\Delta\alpha = (\alpha_2 - \alpha_1), \tag{4.21a}$$

$$\Delta\beta = (\beta_2 - \beta_1), \tag{4.21b}$$

$$\Delta\gamma = (\gamma_2 - \gamma_1), \tag{4.21c}$$

$$\Delta\kappa = (\kappa_2 - \kappa_1), \tag{4.21d}$$

Eqs. 4.18 and 4.17, can be rewritten in matrix form as

$$\begin{bmatrix} \mathbf{r}_{rs}(0) & \mathbf{r}_{rd}(0) & \mathbf{r}_{at}(0) & \mathbf{r}_{ct}(0) & \mathbf{c}_{rs} & \mathbf{c}_{rd} & \mathbf{0} & \mathbf{c}_{ct} \\ \mathbf{r}_{rs}(\tau) & \mathbf{r}_{rd}(\tau) & \mathbf{r}_{at}(\tau) & \mathbf{r}_{ct}(\tau) & \mathbf{0} & \mathbf{0} & \mathbf{0} & \mathbf{0} \end{bmatrix} \begin{bmatrix} \Delta\alpha \\ \Delta\beta \\ \Delta\gamma \\ \Delta\kappa \\ \alpha_2 \\ \beta_2 \\ \gamma_2 \\ \kappa_2 \end{bmatrix} = 0. \tag{4.22}$$

The matrix above shows that

$$\gamma_2 \equiv \text{free parameter}. \tag{4.23}$$

Then finally the algebraic equation for two impulses can be expressed as

$$\begin{bmatrix} \mathbf{r}_{rs}(0) & \mathbf{r}_{rd}(0) & \mathbf{r}_{at}(0) & \mathbf{r}_{ct}(0) & \mathbf{c}_{rs} & \mathbf{c}_{rd} & \mathbf{c}_{ct} \\ \mathbf{r}_{rs}(\tau) & \mathbf{r}_{rd}(\tau) & \mathbf{r}_{at}(\tau) & \mathbf{r}_{ct}(\tau) & \mathbf{0} & \mathbf{0} & \mathbf{0} \end{bmatrix}_{6\times7} \begin{bmatrix} \Delta\alpha \\ \Delta\beta \\ \Delta\gamma \\ \Delta\kappa \\ \alpha_2 \\ \beta_2 \\ \kappa_2 \end{bmatrix} = \mathbf{0}. \tag{4.24}$$

Equation 4.24, shows there is an additional one degree of freedom. This means any of $\Delta\alpha, \Delta\beta, \Delta\gamma, \Delta\kappa, \alpha_2, \beta_2, \kappa_2$, can be selected as the given parameter. Presently κ_2 is selected as the given parameter then,

$$
\underbrace{\begin{bmatrix} \mathbf{r}_{rs}(0) & \mathbf{r}_{rd}(0) & \mathbf{r}_{at}(0) & \mathbf{r}_{ct}(0) & \mathbf{c}_{rs} & \mathbf{c}_{rd} \\ \mathbf{r}_{rs}(\tau) & \mathbf{r}_{rd}(\tau) & \mathbf{r}_{at}(\tau) & \mathbf{r}_{ct}(\tau) & \mathbf{0} & \mathbf{0} \end{bmatrix}}_{\mathbf{A}_2(\tau)} \underbrace{\begin{bmatrix} \Delta\alpha \\ \Delta\beta \\ \Delta\gamma \\ \Delta\kappa \\ \alpha_2 \\ \beta_2 \end{bmatrix}}_{\mathbf{p}_2} = -\kappa_2 \underbrace{\begin{bmatrix} c_{ct_x} \\ c_{ct_y} \\ c_{ct_z} \\ 0 \\ 0 \\ 0 \end{bmatrix}}_{\mathbf{q}_2}, \tag{4.25}
$$

or can be rewritten in compact form as

$$
\mathbf{A}_2(\tau)\mathbf{p}_2 = -\kappa_2\mathbf{q}_2. \tag{4.26}
$$

So two impulses case confers in total two degree of freedom (DOF). It is worth to mention here, from Eq. 4.26, κ_2 can be interpreted as magnification factor which can scale down or up the size of the trajectories in the case of two impulses case.

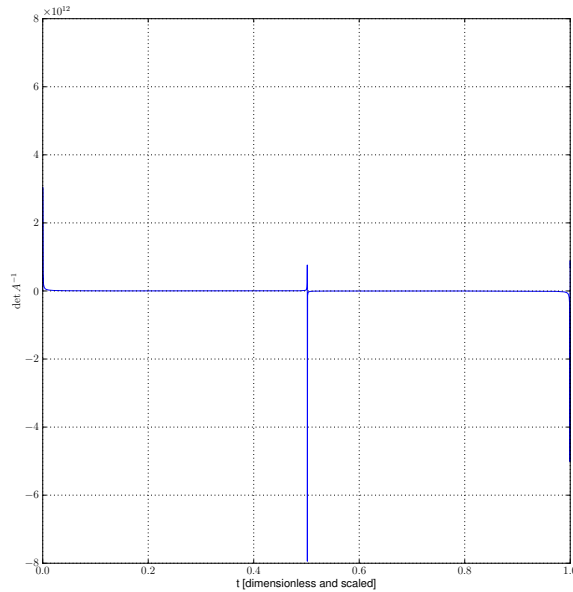Figure 4.4: The value of $|A_2|^{-1}$

Two examples are provided to demonstrate the artificial periodic orbits with two impulses. The first example use $\tau = 0.3T_h$, while γ_2, κ_2 are chosen to be equal with one. Table 4.1 give the obtained parameters for the two connected trajectories. Figures 4.7,4.9,4.11 depict the motions of the two trajectories at each axis respectively. It

appears the two trajectories are close to each other. The values in table 4.1 confirm this result, since the parameters of the trajectories have close values.

Table 4.1: Two Impulses Example Case

Parameters	$\tau = 0.3T_h$	$\tau = 0.5T_h$
α_1	0.0683	-0.7136
α_2	0.0681	0.70
β_1	0.1368	-0.0369
β_2	0.1442	0.0832
γ_1	1.0028	2.3466
γ_2	1.0	1.0
κ_1	1.0062	0.9996
κ_2	1.0	1.0

As a matter of fact, these trajectories are found typical for most of τ. When the value of determinant A_2 plotted against τ as shown in figure 4.4, the determinant has generally small values except when τ is nearby 0, $\frac{T_h}{2}$ and T_h. This causes, with moderate value of κ_2, the parameters between the two trajectories are similar. This is also elaborated by figures 4.5 and 4.6, which show the coeefcients are indeed small within the range of τ previously stated.

Table 4.2: Δv Cost for Two Impulses

	Case 1 (mm/s)	Case 2 (mm/s)
Δv_1	0.0006	0.0417
Δv_2	0.0026	0.0291
Δv_{total}	0.0032	0.0708

The second example, $\tau = \frac{T_h}{2}$, as expected gives a more different trajectories. Figures 4.8, 4.10 and 4.12 shows the two trajectories become more dissimilar. The connected trajectories for the two cases are illustrated in figures 4.15 and 4.16, both for in-plane and out-plane, while the cost of Δv is given by table 4.5.
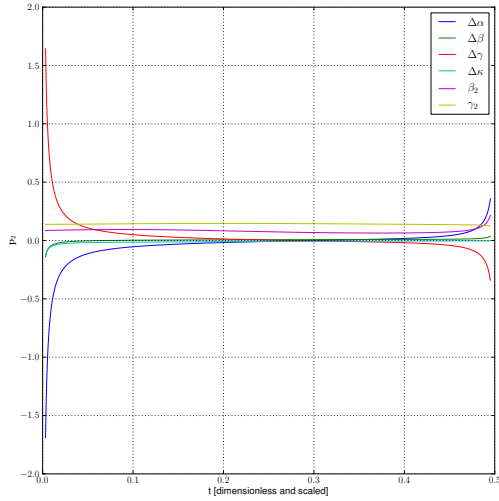
Figure 4.5: $\mathbf{p}_2$ for $0.01\mathrm{T} < \tau < 0.495\mathrm{T}$
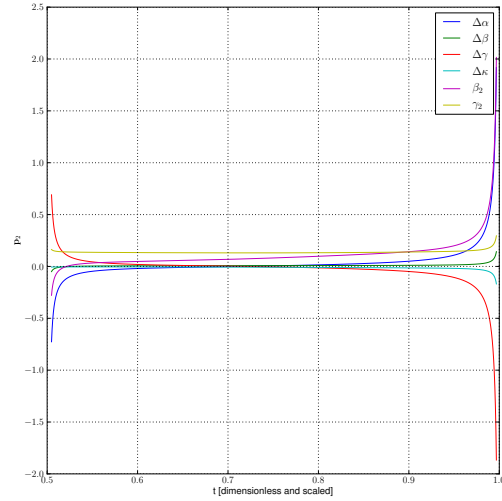
Figure 4.6: $\mathbf{p}_2$, for $0.505 < \tau < 0.99\mathrm{T}$
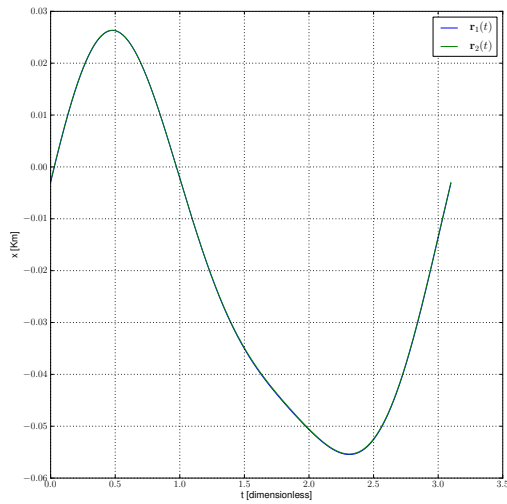
Figure 4.7: Approximated x(t) Case 1
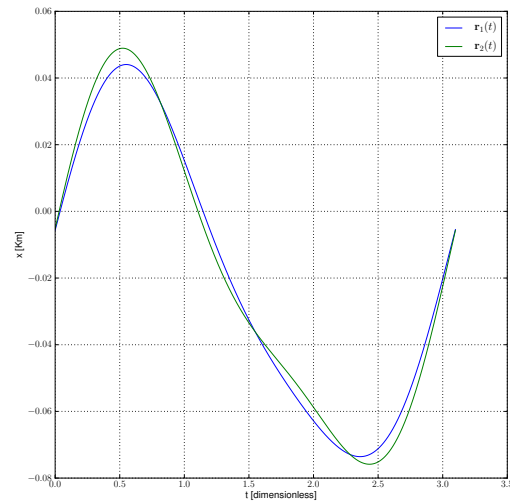
Figure 4.8: Approximated x(t) Case 2
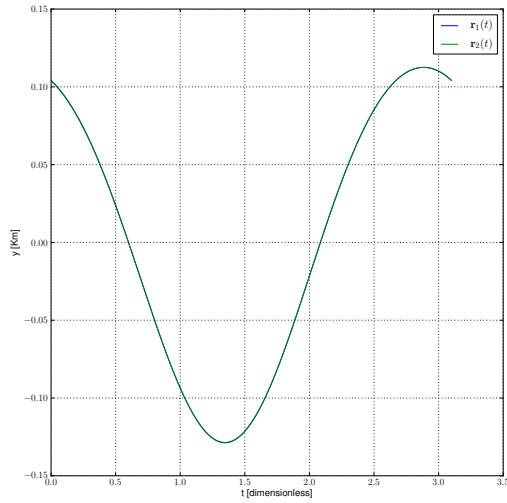
Figure 4.9: Approximated y(t) Case 1

Figure 4.10: Approximated y(t) Case 2

Figure 4.11: Approximated z(t) Case 1

Figure 4.12: Approximated z(t) Case 2

Figure 4.13: In-plane Artificial Periodic Orbit with Two Impulses Case 1

Figure 4.14: In-plane Artificial Periodic Orbit with Two Impulses Case 2
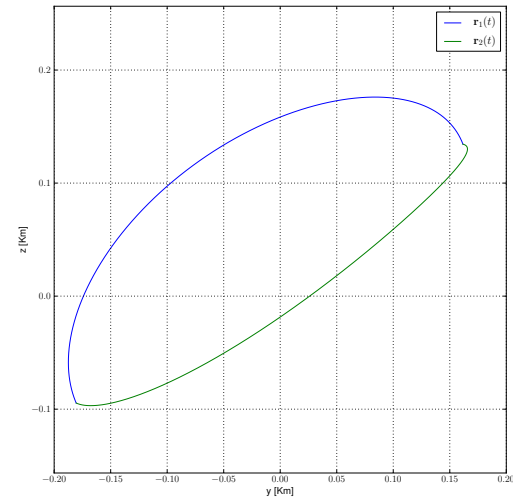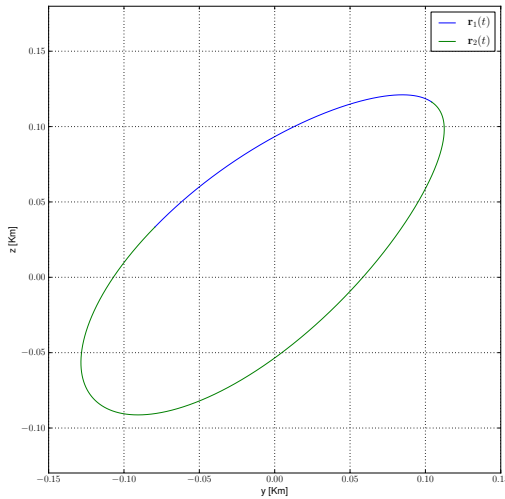
Figure 4.15: Out-plane Artificial Periodic Orbit with Two Impulses Case 1

Figure 4.16: Out-plane Artificial Periodic Orbit with Two Impulses Case 2

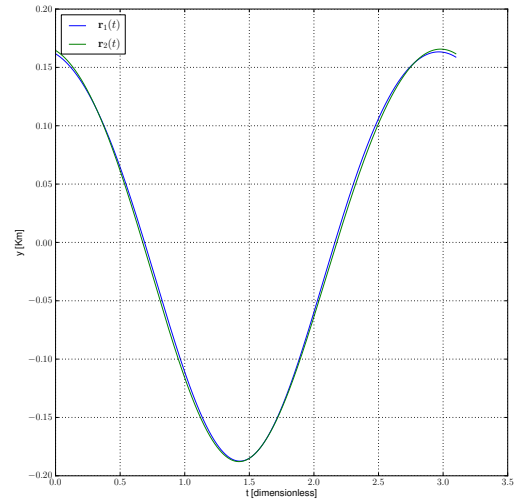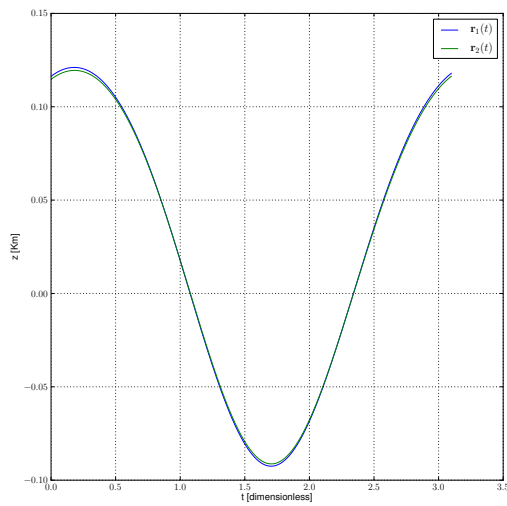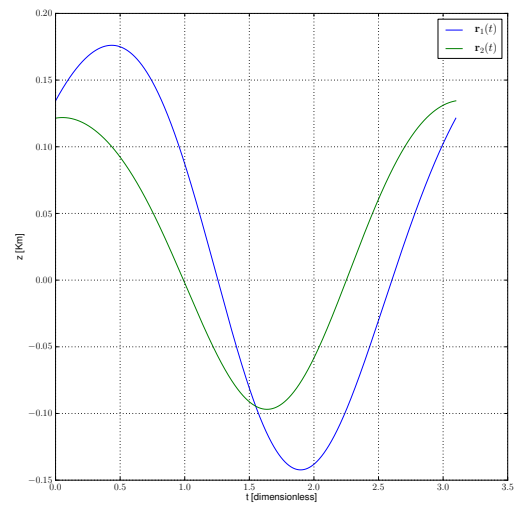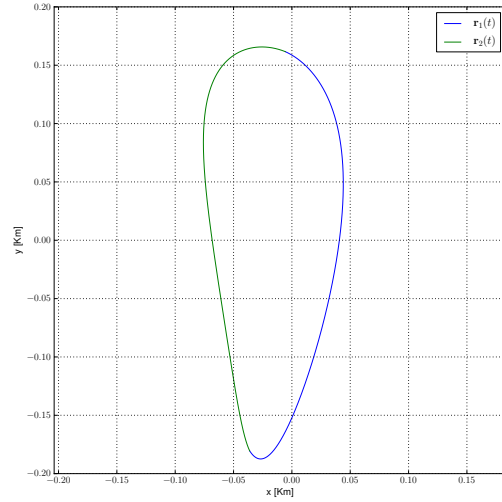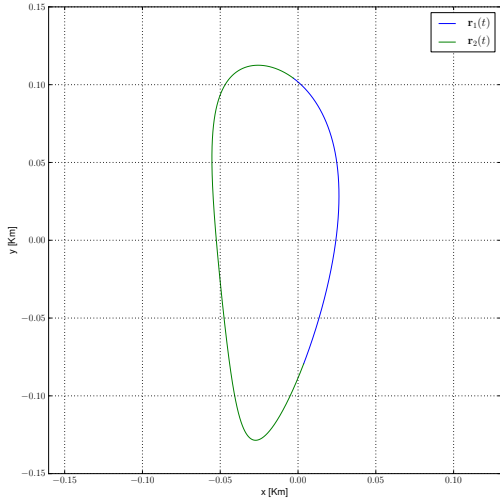## 4.4 Three Impulses Artificial Periodic Relative Motions

The schematic of three impulses is given in Fig. 4.17. In three impulses case, there are two inner connecting points, at τ_1 and τ_2. Based on the schematic figure above,
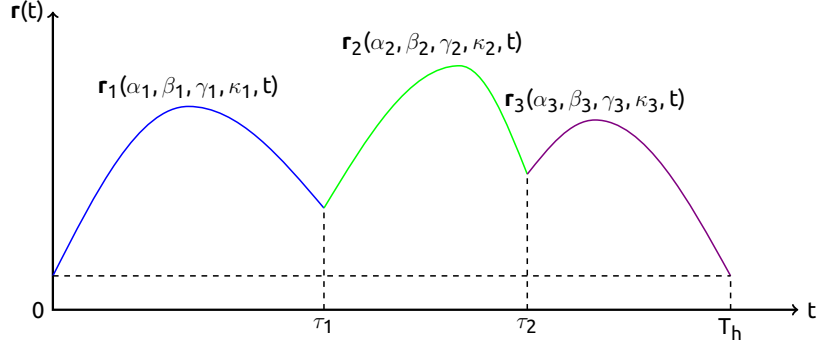
Figure 4.17: Three Impulses Schematic

imposing Eq. 4.1 and Eq. 4.3 for three impulses case yields,

$$\mathbf{r}_1(0) = \mathbf{r}_3(\mathsf{T_h}), \tag{4.27a}$$

$$\mathbf{r}_1(\tau_1) = \mathbf{r}_2(\tau_1), \tag{4.27b}$$

$$\mathbf{r}_2(\tau_2) = \mathbf{r}_2(\tau_2). \tag{4.27c}$$

Expressing each trajectories as function of the linear parameters. Eq. 4.45a, gives,

$$(\alpha_3 - \alpha_1)\mathbf{r}_{\mathsf{rs}}(0) + (\beta_3 - \beta_1)\mathbf{r}_{\mathsf{rd}}(0) + (\gamma_3 - \gamma_1)\mathbf{r}_{\mathsf{at}}(0) + (\kappa_3 - \kappa_1)\mathbf{r}_{\mathsf{ct}}(0) \\ + \alpha_3\mathbf{c}_{\mathsf{rs}} + \beta_3\mathbf{c}_{\mathsf{rd}} + \gamma_3\mathbf{0} + \kappa_3\mathbf{c}_{\mathsf{ct}} = 0, \tag{4.28}$$

Eq. 4.45c,

$$(\alpha_2 - \alpha_1)\mathbf{r}_{\mathsf{rs}}(\tau_1) + (\beta_2 - \beta_1)\mathbf{r}_{\mathsf{rd}}(\tau_1) + (\gamma_2 - \gamma_1)\mathbf{r}_{\mathsf{at}}(\tau_1) \\ + (\kappa_2 - \kappa_1)\mathbf{r}_{\mathsf{ct}}(\tau_1) = 0, \tag{4.29}$$

and Eq. 4.45d,

$$(\alpha_2 - \alpha_1)\mathbf{r}_{\mathsf{rs}}(\tau_2) + (\beta_2 - \beta_1)\mathbf{x}_{\mathsf{rd}}(\tau_2) + (\gamma_2 - \gamma_1)\mathbf{r}_{\mathsf{at}}(\tau_2) \\ + (\kappa_2 - \kappa_1)\mathbf{r}_{\mathsf{ct}}(\tau_2) = 0. \tag{4.30}$$

To make the equation to be more compact, defined,

$$\Delta\alpha_{\mathsf{ji}} = \alpha_{\mathsf{j}} - \alpha_{\mathsf{i}}, \tag{4.31a}$$

$$\Delta\beta_{\mathsf{ji}} = \beta_{\mathsf{j}} - \beta_{\mathsf{i}}, \tag{4.31b}$$

$$\Delta\gamma_{\mathsf{ji}} = \gamma_{\mathsf{j}} - \gamma_{\mathsf{i}}, \tag{4.31c}$$

$$\Delta\kappa_{ji} = \kappa_j - \kappa_i, \tag{4.32}$$

and observing that,

$$\Delta\alpha_{kj} - \Delta\alpha_{ji} = \alpha_k - \alpha_j - \alpha_j + \alpha_i = \alpha_k - \alpha_j. \tag{4.33}$$

The definition is exemplified by

$$\Delta\alpha_{31} - \Delta\alpha_{21} = \alpha_3 - \alpha_1 - \alpha_2 + \alpha_1 = \alpha_3 - \alpha_2 = \Delta\alpha_{32}. \tag{4.34}$$

Considering that

$$\gamma_3 \equiv \text{free parameter}, \tag{4.35}$$

therefore these three equations can rewritten as

$$\begin{bmatrix} \mathbf{L}(0) & \mathbf{c} & \mathbf{0} \\ \mathbf{0} & \mathbf{0} & \mathbf{L}(\tau_1) \\ \mathbf{L}(\tau_2) & \mathbf{0} & -\mathbf{L}(\tau_2) \end{bmatrix}_{9\times 11} \begin{bmatrix} \Delta\mathbf{p}_{31} \\ \mathbf{p}_3 \\ \Delta\mathbf{p}_{21} \end{bmatrix}_{11\times 1} = 0, \tag{4.36}$$

and

$$\Delta\mathbf{p}_{31} = \begin{bmatrix} \Delta\alpha_{31} \\ \Delta\beta_{31} \\ \Delta\gamma_{31} \\ \Delta\kappa_{31} \end{bmatrix}, \tag{4.37}$$

$$\Delta\mathbf{p}_{21} = \begin{bmatrix} \Delta\alpha_{21} \\ \Delta\beta_{21} \\ \Delta\gamma_{21} \\ \Delta\kappa_{21} \end{bmatrix}, \tag{4.38}$$

which can be simplified as

$$\mathbf{p}_3 = \begin{bmatrix} \alpha_3 \\ \beta_3 \\ \kappa_3 \end{bmatrix}, \tag{4.39}$$

where

$$\mathbf{L}(t) = \begin{bmatrix} \mathbf{r}_{rs}(t) & \mathbf{r}_{rd}(t) & \mathbf{r}_{at}(t) & \mathbf{r}_{ct}(t) \end{bmatrix}, \tag{4.40}$$

and

$$\mathbf{c} = \begin{bmatrix} \mathbf{c}_{rs} & \mathbf{c}_{rd} & \mathbf{c}_{ct} \end{bmatrix}. \tag{4.41}$$

This equation in theory has three degree of freedom (DOF). They are the free parameter α_3 and any of two from the other parameters.

To demonstrate the three impulses case, γ_3 and κ_3 as given parameter, then we can write the equation as

$$\begin{bmatrix} \mathbf{L}(0) & \mathbf{c}_{rs} & \mathbf{0} \\ \mathbf{0} & \mathbf{0} & \mathbf{L}(\tau_1) \\ \mathbf{L}(\tau_2) & \mathbf{0} & -\mathbf{L}(\tau_2) \end{bmatrix}_{9\times 9} \begin{bmatrix} \Delta\mathbf{p}_{31} \\ \alpha_3 \\ \Delta\mathbf{p}_{21} \end{bmatrix}_{9\times 1} = -\beta_3 \begin{bmatrix} \mathbf{c}_{rd} \\ \mathbf{0} \end{bmatrix}_{9\times 1} - \kappa_3 \begin{bmatrix} \mathbf{c}_{ct} \\ \mathbf{0} \end{bmatrix}_{9\times 1} \tag{4.42}$$

Table 4.3: Three Impulses Example Case

Parameters	$\tau_1 = 0.4T_h$
	$\tau_2 = 0.6T_h$
α_1	-3.0740
α_2	-0.4301
α_3	2.5387
β_1	0.5402
β_2	1.8945
β_3	1.0
γ_1	6.6484
γ_2	3.8274
γ_3	1.0
κ_1	0.9896
κ_2	0.3358
κ_3	1.0

Table 4.4: Δv Cost for Three Impulses

	(mm/s)
Δv_1	0.1193
Δv_2	0.1210
Δv_3	0.1307
Δv_{total}	0.3710

Defining,

$$\mathbf{A}(\tau_1, \tau_2) = \begin{bmatrix} \mathbf{L}(0) & \mathbf{c}_{rs} & \mathbf{0} \\ \mathbf{0} & \mathbf{0} & \mathbf{L}(\tau_1) \\ \mathbf{L}(\tau_2) & \mathbf{0} & -\mathbf{L}(\tau_2) \end{bmatrix}_{9\times9}, \tag{4.43}$$

In compact form the previous equation above becomes

$$A(\tau_1, \tau_2)\mathbf{p} = -\beta_3 \begin{bmatrix} \mathbf{c}_{rd} \\ \mathbf{0} \end{bmatrix} - \kappa_3 \begin{bmatrix} \mathbf{c}_{ct} \\ \mathbf{0} \end{bmatrix}. \tag{4.44}$$

Hence three impulses case permits increment in degree of freedom compared with the two impulses case so in total there are three DOFs available.

An examples are provided presently, the first example uses $\tau_1 = 0.4T_h$, $\tau_2 = 0.6T_h$. For both this example the design parameters are chosen with values, $\beta_3 = \gamma_3 = \kappa_3 = 1$. The obtained parameters as defined in Eq. 4.44 after solving the algebraic equation are given in table 4.3 and the Δv is shown in table 4.4. Figures 4.18-4.20 display the motion in each axes respectively for the three trajectories and the connected trajectories for in-plane and out-plane respectively are given in figure 4.21 and figure 4.22.
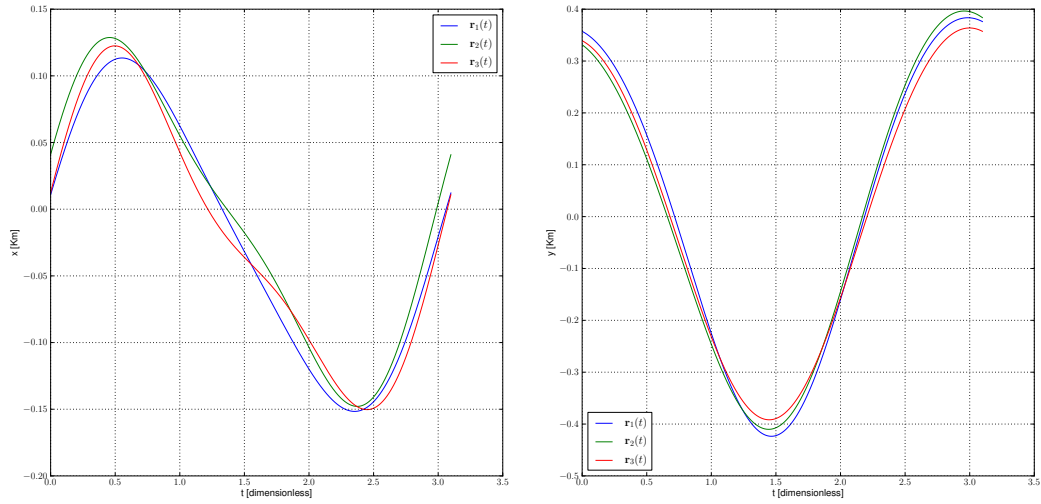
Figure 4.18: Approximated x(t) Three Im-
pulses Case
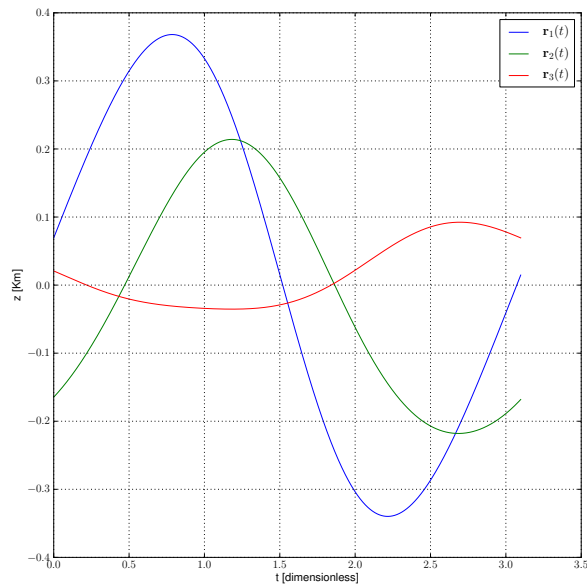
Figure 4.19: Approximated y(t) Three Im-
pulses Case

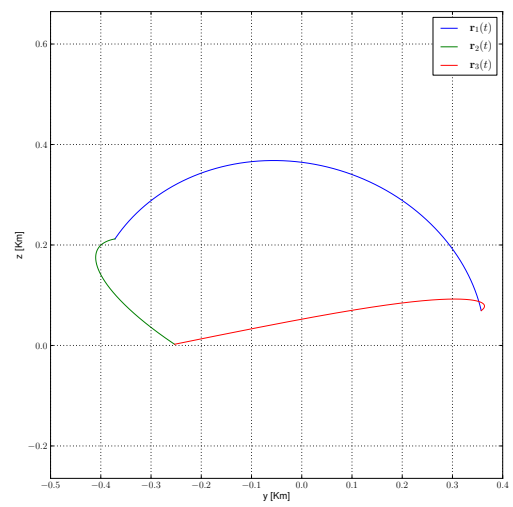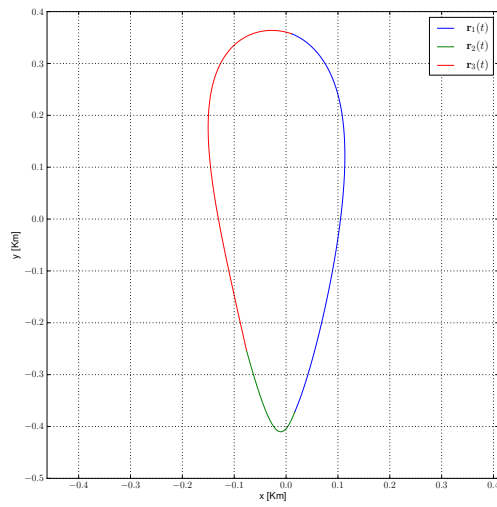Figure 4.20: Approximated z(t) Three Impulses Case

Figure 4.21: In-plane Artificial Periodic Orbit with Three Impulses Case

Figure 4.22: Out-plane Artificial Periodic Orbit with Three Impulses Case
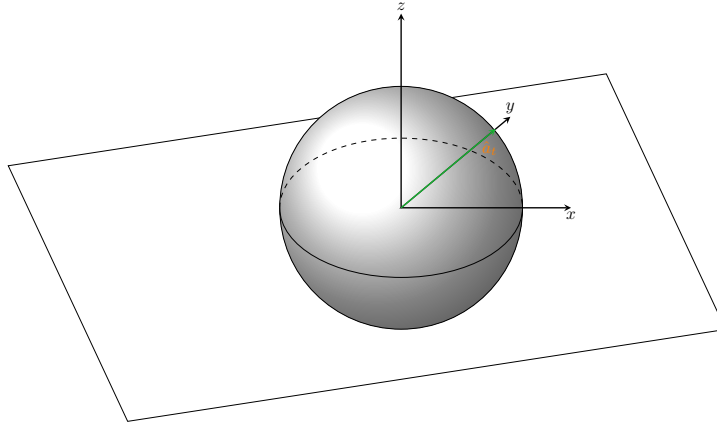
Figure 4.23: Expanded Design Space

4.5 Design Example: Artificial Periodic Relative Orbits with Arbitrary Initial Positions

Natural relative motion in the center manifolds as has been shown, generally only allows one DOF to achieve periodic motions, namely the along-tack direction. Unfortunately this also means that the initial positions of the followers are restricted in one dimension if the followers are expected to periodic. As illustrated in Fig. 4.23, the naturally allowed initial positions are represented by the green line, the along-track direction while other direction within the sphere are prohibited. In order to have initial positions can be arbitrary chosen, additional impulses are introduced accordingly to obtain extra DOF. To maintain the design problem as linear problem, moreover since the main point of this example is to demonstrate the design method when design space expansion is needed, the problem of periodic relative motions with arbitrary initials positions is approached with three impulses. With three impulses the number of linear DOF, excluding connecting times, is three and this is the same number of variables that defines the arbitrary initial positions of a follower spacecraft.

In artificial periodic relative orbits with three impulses case, for connecting the three trajectories, requires,

$$\mathbf{r}_1(0) = \mathbf{r}_0 \tag{4.45a}$$

$$\mathbf{r}_3(T_h) - \mathbf{r}_1(0) = 0 \tag{4.45b}$$

$$\mathbf{r}_2(\tau_1) - \mathbf{r}_1(\tau_1) = 0 \tag{4.45c}$$

$$\mathbf{r}_3(\tau_2) - \mathbf{r}_2(\tau_2) = 0 \tag{4.45d}$$

These four equations can be written in matrix form as,

$$
G(\tau_1, \tau_2)
\begin{bmatrix}
\alpha_1 \\
\beta_1 \\
\gamma_1 \\
\kappa_1 \\
\alpha_2 \\
\beta_2 \\
\gamma_2 \\
\kappa_2 \\
\alpha_3 \\
\beta_3 \\
\gamma_3 \\
\kappa_3
\end{bmatrix}
=
\begin{bmatrix}
r_{0_x} \\
r_{0_y} \\
r_{0_z} \\
0 \\
0 \\
0 \\
0 \\
0 \\
0 \\
0 \\
0 \\
0
\end{bmatrix}
\tag{4.46}
$$

where,

$$
G =
\begin{bmatrix}
rs_x(0) & rd_x(0) & at_x(0) & ct_x(0) & 0 & 0 & 0 & 0 & 0 & 0 & 0 & 0 \\
rs_y(0) & rd_y(0) & at_y(0) & ct_y(0) & 0 & 0 & 0 & 0 & 0 & 0 & 0 & 0 \\
rs_z(0) & rd_z(0) & at_z(0) & ct_z(0) & 0 & 0 & 0 & 0 & 0 & 0 & 0 & 0 \\
-rs_x(0) & -rd_x(0) & -at_x(0) & -ct_x(0) & 0 & 0 & 0 & 0 & rs_x(T) & rd_x(T) & at_x(T) & ct_x(T) \\
-rs_x(0) & -rd_x(0) & -at_x(0) & -ct_x(0) & 0 & 0 & 0 & 0 & rs_y(T) & rd_y(T) & at_y(T) & ct_y(T) \\
-rs_x(0) & -rd_x(0) & -at_x(0) & -ct_x(0) & 0 & 0 & 0 & 0 & rs_z(T) & rd_z(T) & at_z(T) & ct_z(T) \\
-rs_x(\tau_1) & -rd_x(\tau_1) & -at_x(\tau_1) & -ct_x(\tau_1) & rs_x(\tau_1) & rd_x(\tau_1) & at_x(\tau_1) & ct_x(\tau_1) & 0 & 0 & 0 & 0 \\
-rs_y(\tau_1) & -rd_y(\tau_1) & -at_y(\tau_1) & -ct_y(\tau_1) & rs_y(\tau_1) & rd_y(\tau_1) & at_y(\tau_1) & ct_y(\tau_1) & 0 & 0 & 0 & 0 \\
-rs_z(\tau_1) & -rd_z(\tau_1) & -at_z(\tau_1) & -ct_z(\tau_1) & rs_z(\tau_1) & rd_z(\tau_1) & at_z(\tau_1) & ct_z(\tau_1) & 0 & 0 & 0 & 0 \\
0 & 0 & 0 & 0 & -rs_x(\tau_2) & -rd_x(\tau_2) & -at_x(\tau_2) & -ct_x(\tau_2) & rs_x(\tau_2) & rd_x(\tau_2) & at_x(\tau_2) & ct_x(\tau_2) \\
0 & 0 & 0 & 0 & -rs_y(\tau_2) & -rd_y(\tau_2) & -at_y(\tau_2) & -ct_y(\tau_2) & rs_y(\tau_2) & rd_y(\tau_2) & at_y(\tau_2) & ct_y(\tau_2) \\
0 & 0 & 0 & 0 & -rs_z(\tau_2) & -rd_z(\tau_2) & -at_z(\tau_2) & -ct_z(\tau_2) & rs_z(\tau_2) & rd_z(\tau_2) & at_z(\tau_2) & ct_z(\tau_2)
\end{bmatrix}
\tag{4.47}
$$

and the arbitrary initial positions are defined as

$$
\mathbf{r}_0 =
\begin{bmatrix}
r_{0_x} \\
r_{0_y} \\
r_{0_z}
\end{bmatrix}
\tag{4.48}
$$

Let see an example below to demonstrate the design method. The initial positions used in this example are

$$
\mathbf{r}(0) = \mathbf{r}(T) =
\begin{bmatrix}
1 \\
1 \\
-2
\end{bmatrix}
\text{Km}
\tag{4.49}
$$

Obviously the Δv's that must be given are a function of the connecting times, τ_1, τ_2, and hence the matrix $G(\tau_1, \tau_2)$ consequently. Despite the relative motions are linear in term of the constant parameters, but inherently they are nonlinear function of the connecting times.

The optimization process in finding the total Δv, can be carried out numerically. For this case, the minimum Δv is obtained as shown in Table 4.5. As comparison Table 4.6 gives total Δv if $\tau_1 = \frac{1}{3}T$, $\tau_2 = \frac{2}{3}T$ are used as the connecting times.

The column at each of the tables, labeled as 2nd Order are results obtained when the basic motions, or the fundamental set solutions are given by the approximation, while the nonlinear column are results when the basic motions are fully nonlinear. In artificial

Table 4.5: Optimum Δv for Arbitrary Initial Positions

	2nd Order	Non Linear
τ_1	0.8496	0.8496
τ_2	2.2489	2.2489
Δv_{total} (mm/s)	4.3753	3.3395

periodic relative motions with impulsive control, the DOF is not changed when higher order of approximation is used. While using 2nd Order Fourier series approximation offers easier numerical computation, but going to higher order even up to fully nonlinear basic motions, found using numerical propagation of the bases, doesn't add complexity in computation or influence the DOF since the value of matrix **G** is the connecting points.

Table 4.6: Δv for Arbitrary Initial Positions ($\tau_1, \tau_2 = 0.25T, 0.75T$)

	2nd Order	Non Linear
Δv_{total} (mm/s)	4.7279	3.5866

If the results from the 2nd Order approximation and the nonlinear compared, the total Δv are certainly different even when the optimum connecting times are not much different. This happens due to the velocity components of the fundamental set solutions are not perfectly approximated using only 2nd Order approximation, thus give different Δv. However the 2nd Order approximation doesnt't give exagerated results either, hence still useful to predict rough Δv to attain the periodicity. The resulted trajectories are given in Figures 4.24, 4.25 and 4.26. The combined in-plane and out-plane are given in Figures 4.27 and 4.28.

4.6 Nonlinear effects

As presented in previous section, the proposed design method succeeded to achieve artificial periodic relative orbits with impulsive control for arbitrary initial positions case. It's important to highlight again here that the degree or approximation of the fundamental set solutions doesn't reduce or add DOF to the design but improve the accuracy of the results when tested in full nonlinear environment. However since the fundamental set solutions are obtain from nonlinear propagation of the extracted bases from the monodromy matrix, it's reasonable to check if the bases are free from the non periodic modes, the divergent and convergent motions. Furthermore the Δv and the connecting times, e.g. τ_1, τ_2 should be checked as well to see nonlinear effects.

Solving Eq. 4.46, gives the design parameters, $\alpha_n, \beta_n, \gamma_n$ and κ_n, at certain τ_1, τ_2, in the example optimal values were used, and consequently initial positions and the Δv to be applied. Figures 4.29 and 4.30 show the in-plane and out-plane motions, labeled with NLP (nonlinearly propagated), where initial positions from the design requirements, the
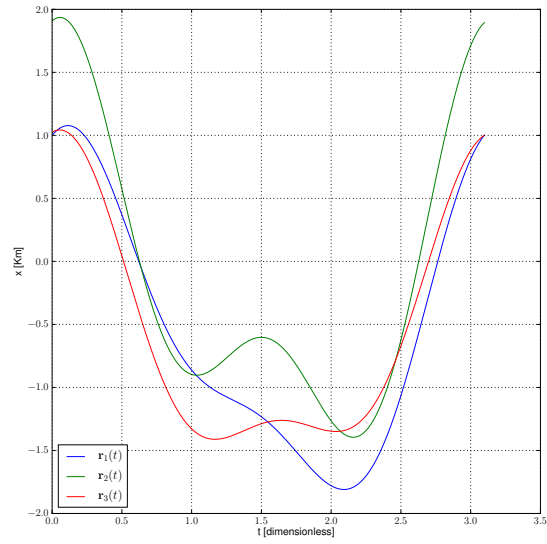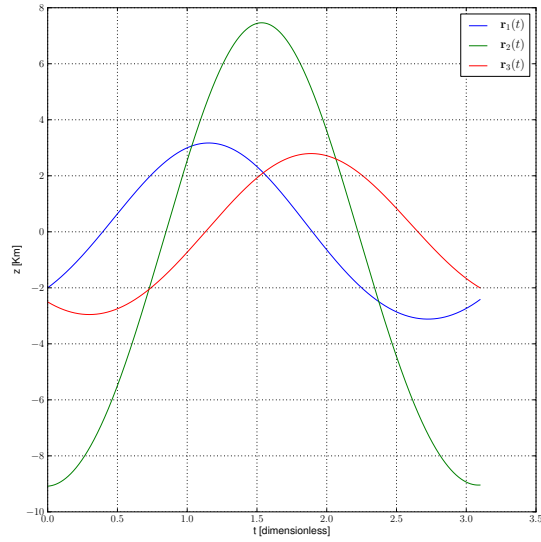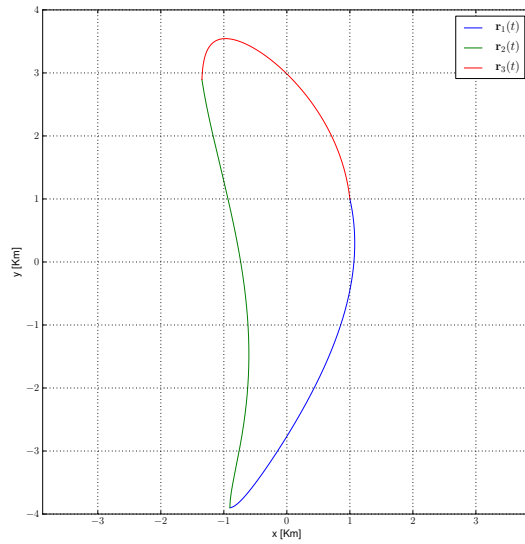
Figure 4.24: x(t)
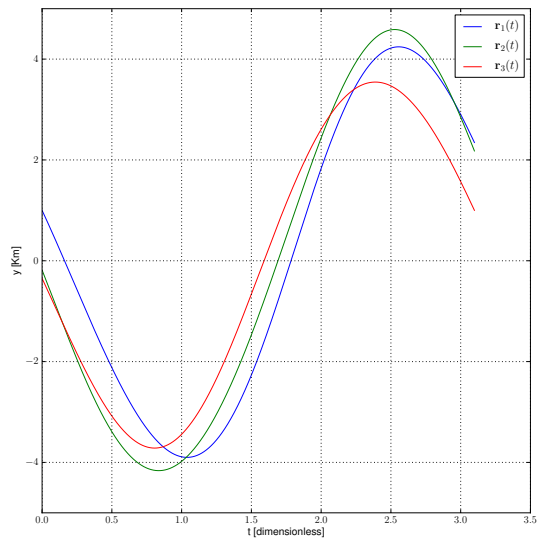
Figure 4.25: y(t)

Figure 4.26: z(t)

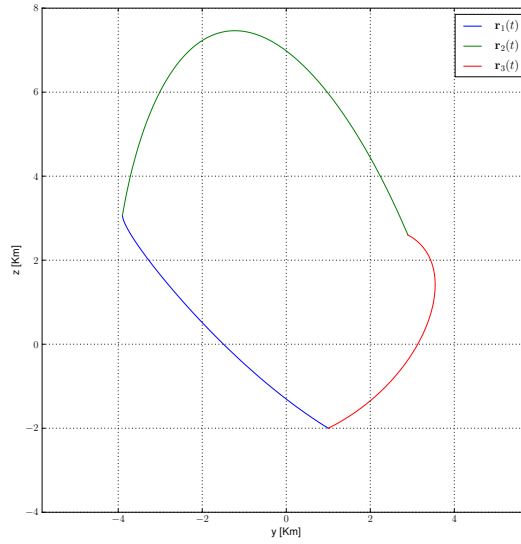Figure 4.27: In-plane of the approximated motion

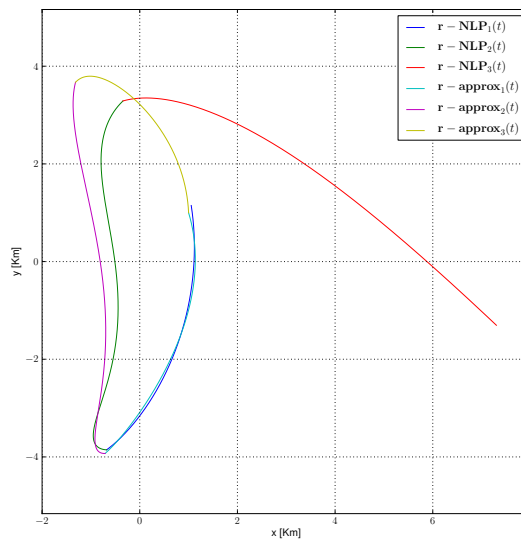Figure 4.28: Out-plane of the approximated motion

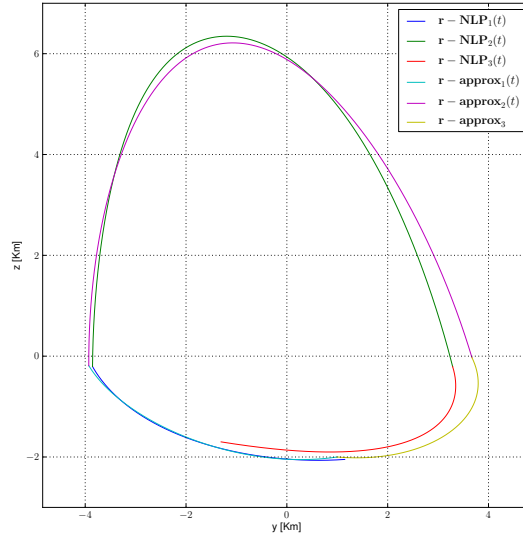Figure 4.29: In-plane motion with initial from the bases

Figure 4.30: Out-plane motion with initial from the bases

design parameters calculated from 2^{nd}Order approximation and initial velocities from the bases in Table 3.2. The figure indicate that the nonlinearly propagated motion doesn't comply with the approximated motions. This is due to two things, difference in initial positions, and Δv found using the approximation. This figure doesn't present nonlinear effects per se, but shows the limitation of the 2^{nd}Order approximation for calculating initial state vectors, thus include the non-periodic modes. If the initials state vectors fully from the approximations, Eq 3.10, the nonlinearly propagated results shows larger deviation than the obtained results in Figures 4.27 and 4.28, as shown in Figures 4.31 and 4.32. The fact that the approximated fundamental set solutions doesn't model the initial state vectors accurately is contrasted when the design parameters and the bases are used to get the positions and velocities at initial point in Figures 4.33 and 4.34. In this two figures, although the combined relative motions aren't connected, the non-periodic modes however are ruled out.

There are two approach to improve the results in Figures 4.33 and 4.34, either introducing Δv correction at τ_2 and T like Fixed Time Arrival (FTA) technique or improving accuracy of the approximation model. The latter are shown here, since it corresponds on inspecting the bases of the center manifolds free from the non-periodic modes and also from practical point of view, the full non linear are already made available during establishing the approximation model in Chapter 3. When the fundamental set solutions used in finding matrix **G** are the full nonlinear ones, the linear combination of the fundamental set solutions (FSS) and the initial state vectors, τ_1, τ_2 and Δv_1, Δv_2 are perfectly in agreement as provided in Figures 4.35 and 4.36. This suggests that bases only contain the periodic motions, free from both the convergent and the divergent modes and the nonlinear effects can be safely ignore as long as the size of the formations are

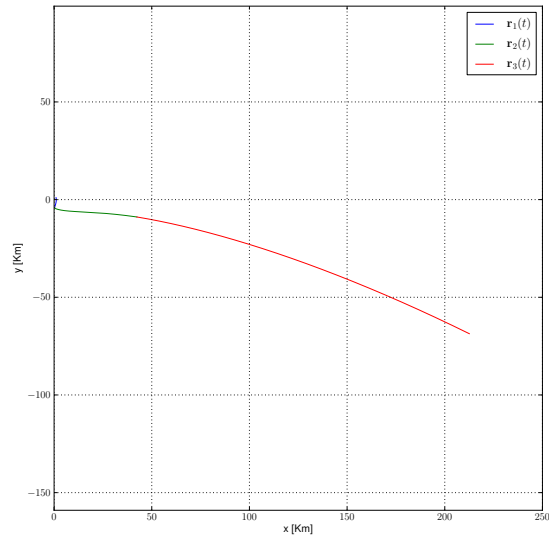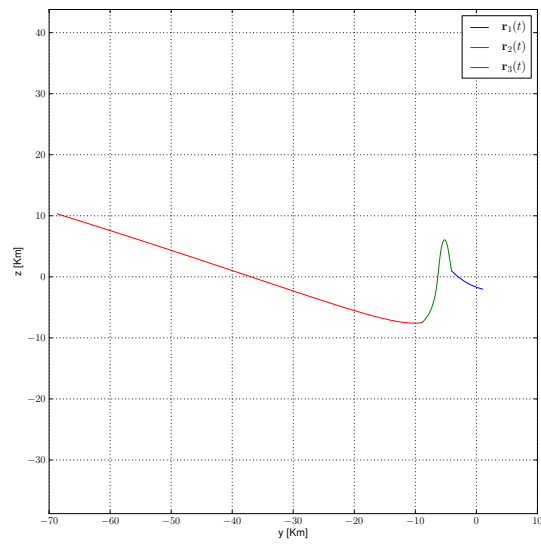Figure 4.31: In-plane motion with initial from the approximations

Figure 4.32: Out-plane motion with initial from the approximations

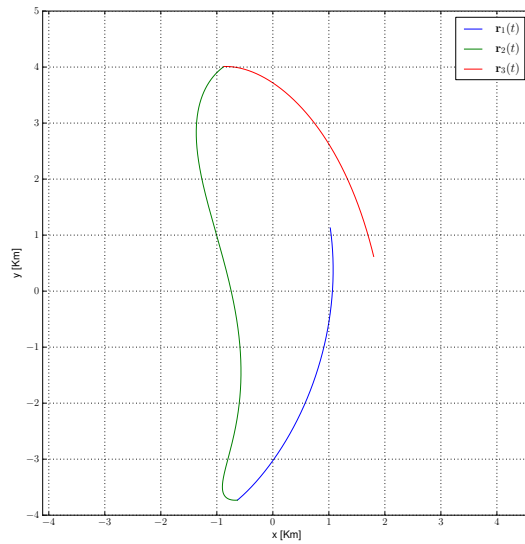kept significantly smaller than the size of the halo orbits.

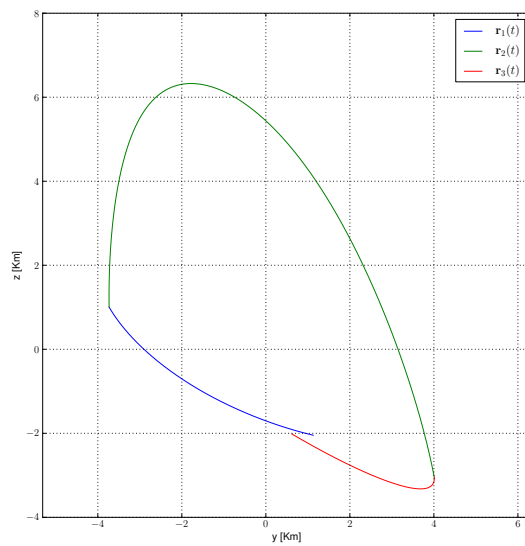Figure 4.33: In-plane motion with initial from the bases

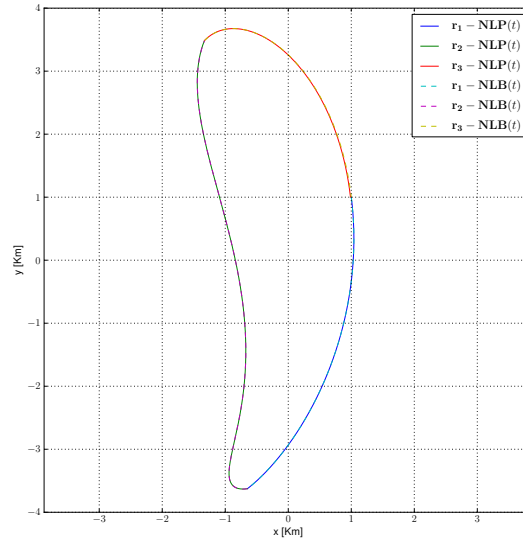Figure 4.34: In-plane motion with initial from the bases

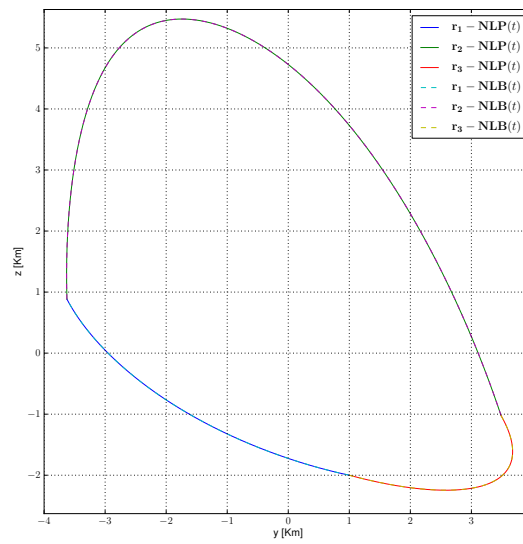Figure 4.35: In-plane motion with full nonlinear FSS

Figure 4.36: Out-plane motion with full nonlinear FSS

CHAPTER 5

Concluding Remarks

Contents

In this thesis design of loose formation flying around halo orbits has been presented. The design address two types of formations, natural loose formations and periodic loose formations with impulsive control. The proposed design method is established by confining the relative motion within the center manifolds to nullify the converging and the diverging components of the follower spacecraft. Thanks to the extracted bases based on the Monodromy matrix, we have managed to treat the relative motion as linear combination of the fundamental set solutions with constant coefficients α, β, γ and κ. Additional importance of using the bases obtained is also obvious since the bases are not simply independent directions but they also intentionally constructed to have geometrical interpretations hence help to visualize the design process.

For natural formations two modes of motion, long-term and short-term, were identified. It was discovered that the long-term motion could be approached as a discrete mapping for the $n-th$ period and that the short-term motion could be fitted well with modified Fourier series having an additional linear term. This thesis has shown how the proposed design method transforms the formation design problem from the domain of differential equations to that of algebra. This makes solution of the design problem simpler and, moreover, allows long-term and short-term motion to be treated simultaneously or independently. The validity of the proposed design method was demonstrated in a set of example problems which involved both long-term and short-term motion.

Natural loose formation however only allows limited space in designing formations. To remedy this lack of degree of freedom, impulsive control is introduced. Impulsive control is used to achieve artificial periodic relative motions that loosely controlled. It was found by adding the number of impulsive control, the degree of freedom does increase. In single impulsive the solution is only the trivial while in two and three impulsive cases, the nontrivial solutions are also available. Numerical examples were given to demonstrate the concept of the design of periodic loose formations proposed in this thesis. Although only elaborated in up to three impulses, basically the systematic design is expandable to larger number of impulses. The nonlinear basic motions can be utilized to obtained trajectory for artificial periodic orbits with better accuracy. Second order approximation is insufficient to model the initial state for periodicity hence may contain the convergent motions, but still can utilized as approximation model and used FTA to enhance the accuracy and correct the velocity.

5.1   Recommended Future Works

There are two subjects recommended for future works.

- Fuel cost optimization for artificial periodic loose formations. As has been shown, for the cases where number of impulses larger than 2, the time, τ, where the impulsive control is exerted can be selected as desired. Addition to the variation of the design parameters, τ, also influences the magnitude of Δv cost. Study on how these parameters interact locally or globally, will elucidate the optimum fuel cost for maintaining periodic loose formation in the vicinity of Halo orbits.

- Formation insertion and deployment. How to deploy the loose formation is also an important aspect in bringing the loose formation in the nearby Halo orbits to come into reality. Various aspects, such as on board navigation and control instruments, orbit determination and scientific tasks must be discussed wholly and in detail.

- Study on eccentricity effects is also important to address and including other sources of perturbation forces will bring this study closer into real practice in future space missions.

Bibliography

[Clohessy 1960] WH Clohessy and RS Wiltshire. *Terminal guidance system for satellite rendezvous*. Journal of the Aerospace Sciences, vol. 27, no. 9, pages 653–658, 1960. (Cited on page 1.)

[Connor Howell 1984] K. Connor Howell. *Three-dimensional, periodic, halo orbits*. Celestial Mechanics and Dynamical Astronomy, vol. 32, no. 1, pages 53–71, 1984. (Cited on page 6.)

[Farquhar 1968] R. W. Farquhar. *The Control and Use of Libration-Point Satellites*. PhD thesis, Stanford University, 1968. (Cited on page 1.)

[Folta 2004] D. Folta, K. Hartman, K. Howell and B. Marchand. *Formation control of the maxim L2 libration orbit mission*. In AIAA/AAS Astrodynamics Specialist Conference, August 12–18, 2004. (Cited on page 2.)

[Gill 2004] E. Gill and H. Runge. *Tight formation flying for an along-track SAR interferometer* 1. Acta Astronautica, vol. 55, no. 3-9, pages 473–485, 2004. (Cited on page 2.)

[Gomez 2001] G. Gomez, J. Llibre, R. Martines and C. Simo. Dynamics and mission design near libration points, volume 2 of *World Scientific Monograph Series in Mathematics*. World Scientific, 2001. (Cited on page 9.)

[K. C. Howell 2003] B. G. Marchand K. C. Howell. *Control Strategies for Formation Flight in the Vicinity of the Libration Points*. Advances in the Astronautical Sciences, vol. 114, no. 1, pages 197–230, 2003. (Cited on page 2.)

[Koon 2008] W.S. Koon, M.W. Lo, J.E. Marsden and S.D. Ross. Dynamical systems, the three-body problem and space mission design. Marsden Books, 2008. (Cited on page 9.)

[Kyle T. Alfriend 2010] Pini Gurfil Kyle T. Alfriend Srinivas R. Vadali and Loius Berger. Spacecraft formation flying. Elsevier, 2010. (Cited on page 2.)

[Marchal 1989] C. Marchal. The Three Body Problem. Elsevier, 1989. (Cited on page 9.)

[Roberts 2005] J.A. Roberts. *Satellite formation flying for an interferometry mission*. PhD thesis, Cranfield University, 2005. (Cited on page 2.)

[Scharf 2005a] D.P. Scharf, F.Y. Hadaegh and S.R. Ploen. *A survey of spacecraft formation flying guidance and control. Part II: Control*. In American Control Conference, 2004. Proceedings of the 2004, volume 4, pages 2976–2985. IEEE, 2005. (Cited on page 1.)

[Scharf 2005b] D.P. Scharf, F.Y. Hadaegh and S.R. Ploen. *A survey of spacecraft formation flying guidance and control. Part I: Dynamics*. In American Control Conference, 2004. Proceedings of the 2004, volume 4, pages 2976–2985. IEEE, 2005. (Cited on page 1.)

[Strang 2003] G. Strang. Introduction to linear algebra. Wellesley Cambridge Pr, 2003. (Cited on pages 9 and 16.)

[Szebehely 1967] V. Szebehely. Theory of orbits. Academic Press New York, 1967. (Cited on page 5.)

[Weintraub 2008] S.H. Weintraub. Jordan canonical form: application to differential equations. Morgan & Claypool, 2008. (Cited on page 9.)

Nomenclature

D   Jacobian matrix

J   Jordan canonical form

M   Monodromy matrix

T   Halo orbit's period

$\hat{e}$ Generalized eigenvector

$\mathbf{e}$ Eigenvector or basis

$\mathbf{x}$ State vector of the relative motion

Φ State transition matrix

α Design parameter in the rot-sum direction

β Design parameter in the rot-diff direction

δ Scaling factor for linear region

γ Design parameter in the along-track direction

κ Design parameter in the cross-track direction

λ Eigenvalue

μ Mass ratio

$\mathbf{X}$ State vector of the reference trajectory

E   Subspace

Design of Loose Spacecraft Formation Flying around Halo Orbits

-Abstract-

Two spacecraft or more are assumed to be in a state of loose formation flying around a collinear Lagrangian point in the Sun-Earth Circular Restricted Three-Body Problem (CRTBP) system. The orbit reference of choice for the leader is a Halo orbit and the followers are assumed to follow nearby and be constrained either geometrically or in size. This type of formation could be useful in the future for constructing space ports, space telescopes, astronomical spacecraft requiring sun shields and, with greater numbers, spacecraft swarm missions. The formation design method is constructed by firstly seeking the local coordinate system from the monodromy matrix through extraction of the independent bases which span the space of the Halo orbit. To nullify diverging and converging motion, we confine the relative motion to within the periodic subspaces. Two types of formations are studied in this thesis, natural loose formations and periodic loose formations with impulsive control. For natural formations, two modes of relative motion within these subspaces, long-term and short-term motions. In this study, the long-term motion is approximated by deriving a discrete formulation of independent directions based on the eigenvectors of the monodromy matrix, while for the short-term motion the fundamental set solutions are modeled using Fourier series and additional linear functions. Since the size of the formation discussed is significantly smaller than that of the Halo orbit, the formation design method can fundamentally be stated as a process of linearly combining these approximations to achieve the desired formation. Consequently, use of this approach transforms formation design from a differential equation problem into an algebraic one, and furthermore enables the long-term and short-term motion design problems to be handled either jointly or separately. To increase design degree of freedom impulsive control is introduced to the formation problem. The use of single, two and three impulses are specially discussed in detail. Design examples, both for natural and with impulsive control formation are presented to demonstrate the validity of the design method. **Keywords:** Restricted Circular Three-Body Problem, Loose Formation Flying, Halo Orbits, Impulsive Control